NTNU – Trondheim
Norwegian University of
Science and Technology

A rangefinder for measuring vibrations of structures

Optical-FMCW interferometry

Lars Christian Eriksson
Grodås

Master of Science in Electronics
Submission date: August 2014
Supervisor: Ulf Lennart Østerberg, IET
Co-supervisor: Astrid Aksnes, IET
                          Jon Kristian Hagene, Norsk Elektro Optikk AS

Norwegian University of Science and Technology
Department of Electronics and Telecommunications

Problembeskrivelse

Bakgrunn:

Norsk Elektro Optikk har gjennom ISTIMES og et studentprosjekt laget et system for å måle vibrasjoner på bygningskonstruksjoner som broer. Dette for å kunne overvåke strukturens svingninger som gjør det mulig å oppdage forandringer som tyder på skade på strukturen. I prosjektoppgaven ble et måleinstrument som målte bevegelsen til et objekt i X og Y planet implementert. Systemet kunne finne XY-posisjonen med en nøyaktighet omkring 0.1 mm. Det er av interesse å legge til måling av Z posisjon i tillegg til X og Y.

Gjennomføring:

Denne oppgaven tar sikte på å måle avstanden til et objekt, Z, ved å utvikle en ny modul for dette formålet. Både absolutt avstand innenfor noen cm og små vibrasjoner på mindre enn 1 mm er av interesse. Årsak er at små bevegelser er innenfor bygningskonstruksjonens bruksområde. Konstruksjonen vil svinge ved sin egenfrekvens når den utsettes for ulike laster som trafikk og vind. Store begevelser kan komme av temperaturforandringer, men kan også indikere at konstruksjonens bruksgrense er overskredet, slik at man når bruddgrensen. I dette tilfellet bør konstruksjonen undersøkes for skade. Egenfrekvensen til store strukturer er ofte lav og vil i denne oppgaven forventes å ligge mellom 1-10 Hz. Modulen som blir konstruert i denne oppgaven vil være selvstendig, men en senere del av prosjektet kan bli å integrere de to systemene til et større system som måler både X, Y og Z posisjon. Det er ønskelig å gjøre dette på en fornuftig kostnads/kompleksitetsnivå.

Masteroppgaven vil være både teoretisk og praktisk:

- Identifisere eksisterende løsninger for måling av avstand og vibrasjoner gjennom et litteraturstudium.
- Vurdere hvilken metode som passer best/er mest praktisk for dette prosjektet.
- Konstruere en prototype og karakterisere komponentene for å finne begrensninger.
- Gjøre forbedringer for å nå målet på cm-oppløsning på avstandsmålingen og bedre enn 1 mm på vibrasjoner mellom 1-10 Hz.

Abstract

The optical Frequency Modulated Continuous Wave (FMCW) technique along with utilizing the Doppler shift was investigated for the application of monitoring distance to and oscillation of a bridge. The equipment was borrowed from Norsk Elektro Optikk AS (NEO). The importance of coherence length and linearity of scan when a laser is tuned was encountered, both presenting a challenge to achieving a high signal to noise (SNR) level. Two lasers were tested in the optical FMCW setup, with coherence length of 15 m and 150 m, respectively. The laser with the shortest coherence length only had a detectable signal to a distance of less than 3 m. With the other laser measurements up to 15 m were done, and a signal was detected up to 20 m. The suitability of the system for detecting vibrations was tested by mounting a retroreflector on a large speaker, and oscillating this at low frequencies, comparable to typical vibration of bridges(a few Hz, with amplitude of mm-cm). The Doppler shift induced by a velocity of 0.01 m/s was approximately 13 kHz. As an example, this makes it possible to measure bridge oscillations with a frequency 4 Hz, with a peak to peak displacement of 0.1 mm, when presuming a sinusoidal movement of the bridge. The resolution of the absolute distance is calculated to be 2 cm for this setup if the detection of a change in the beat frequency of 1.58 kHz is possible. The modulation frequency of 300 Hz enables rapid sampling which poses no limit to measure oscillations of structures up to 10 Hz.

The system proposed still needs some work: linearise the wavelength scan of the laser, change the detector to one with a much higher bandwidth and create a signal processing back end to calculate the distance and amplitude/frequency from the signal. Other optical components, such as the lenses, retroreflectors and the beamsplitter, need to be replaced with ones that are optimized for the wavelength of the laser.

Sammendrag

Optisk Frequency Modulated Continuous Wave (FMCW) ble undersøkt og testet for å kunne overvåke forflyttning og vibrasjon av broer. Utstyret ble lånt fra Norsk Elektro Optikk AS (NEO). Viktigheten av koherenslengde og lineære scan når strømmen til laseren blir modulert ble oppdaget, noe som er svært viktige for å få et godt signal-til-støy forhold. To lasere ble testet i oppsettet, en med koherenslengde på 15 m, og en med koherenslengde på 150 m. Laseren med kort koherenslengde resulterte i at signalet ikke kunne detekteres ved en avstand på 3 m. Laseren med lang koherenslengde ble brukt til målinger opp til 15 m, og et svakt signal ble detektert opp til 20 m. Systemet ble testet for å detektere vibrasjoner ved å montere en retroreflektor på en stor høytaler, som ble påtrykt et signal på 0.5 Hz, som er sammenlignbart med eller lavere enn typiske vibrasjoner i broer. Dopplerskiftet fra en hastighet på 0.01 m/s var omtrent 13 kHz. Som et eksempel gjør dette det mulig å måle brooscillasjoner på 4 Hz, med et top-til-top utslag på 0.1 mm detekterbar, om man forutsetter sinus-form på bevegelsen. Oppløsningen til den absolutte avstanden ble kalkulert til omtrent 2 cm for dette oppsettet, dersom det er mulig å detektere en forandring i sveve(beat) signalet på 1,58 kHz. Modulasjonsfrekvensen på 300 Hz gjør det mulig å sample raskt, som ikke legger noen begrensning på muligheten til å måle brooscillasjoner på opp til 10 Hz.

Systemet som er foreslått her trenger videre arbeid: linearises bølgelengdeskannet til laseren, erstatte detektoren med en med større båndbredde og lage en signalbehandlings back-end for å beregne avstanden og hastigheten/vibrasjonen ut fra signalet. De resterende optiske komponentene, som linsene, retroreflektorene og beamsplitteren, bør også byttes med komponenter som er optimalisert for bølgelengden til laseren.

Preface

I would like to thank my supervisors Astrid Aksnes and Ulf-Lennart Öster-berg, who set aside their valuable time to guide me through the masters thesis. I also want to thank my external supervisor Jon Kristian Hagene and Norsk Elektro Optikk AS for helping me when when I faced difficulties and supplying equipment and helping me customise parts when needed. This thesis was very challenging, in part due to me underestimating the challenges of building optical setups, but I am glad that I chose this subject because of all the new knowledge I have obtained about laser ranging and interferometry, and all the practical laboratory experience I have gained.

Abbreviations & Definitions

Abbreviations

BS   Beamsplitter

f_{if} Intermediate frequency

FMCW Frequency Modulated Continuous Wave

LDV   Laser Doppler Vibrometer

M   Mirror

VCSEL Vertical cavity surface emitting laser

x

List of Figures

Contents

Chapter 1

Introduction

1.1 Monitoring structural health

For monitoring the health of structures one can monitor the structures vibrations over time to detect changes to the structure. Monitoring structures health is very important because of the consequences to human life and the financial loss if structures like a bridge were to fail. It is also challenging to correctly calculate the strength a bridge needs to withstand extreme wind conditions or unforeseen damages to the structure, and still be in use for many decades. The Norwegian Public Roads administration (Statens Vegvesen) has mentioned these challenges several times in [1]. Therefore it is interesting to monitor the actual oscillation of a structure in use, so that it is possible to verify the health of the structure. The monitoring of vibrations can be solved with many different techniques. One way to do this was covered in my project thesis, *Optical Displacement Monitoring*, which was based on image processing of the raw images from a camera. This technique could detect movement in the horizontal or vertical direction in relation to the camera. If X and Y corresponds to horizontal and vertical movement, then the movement in the Z direction is movement towards and away from the camera. This movement is not measured by the system. To improve the system,

this dimension is desired to be included, with the following specifications:

- Operating distance up to 25-30 m.

- Distance resolution of some cm.

- Vibration resolution of less than 1 mm for vibrations of 1-10 Hz.

- Sampling rate of position fast enough to monitor vibrations of 10 Hz.

Building a system that meets these requirements is the theme of my masters thesis.

1.2   Distance measurement suitable for Structural Health Monitoring

Distance measurement done by electronic systems has been possible the last century. The first techniques were based on radio waves. Lasers were applied to distance measurements soon after their invention, and systems for range measurements were invented shortly thereafter [2]. There are many overview articles that cover the different methods of measuring distance with the use of a laser [3] [4] [5]. One such method is the triangulation method, which takes advantage of a separation between the image detector and the laser projector to find an angle of the reflected light which corresponds to the amplitude in the Z direction. Some techniques require access to the structure, like placing a fiber in/on the structure to measure strain and vibrations [6]. Others techniques like Electronic Speckle Pattern Interferometry/TV-holography and Electronic Shearography are capable of measuring a larger surface continually to perform vibration measurements and strain measurements [7]. The main techniques can be divided into the time-of-flight family and the interferometer family. Time-of-flight techniques measure the time between a transmitted signal and a received signal to determine the distance. This can for example be done by sending a pulse of laser light at t=0 and counting the time until the pulse is reflected back. One such system is designed by [8], and

can operate with a total error of ± 2 mm and a single shot precision better than 5.1 mm. The working distance is up to 34.5 m. To measure smaller displacements than this interferometric methods can be suitable.

Interferometer measurements are done by comparing the interference between two electric fields. The two fields are superposed in some interferometer setup like Michelson, which is the most common interferometer setup. These setups can detect very small differences in path length by comparing the phase difference between the two beams, but in its simplest form this technique cannot measure static distances. But by modulating or scanning the wavelength of the laser, the absolute distance difference in the two arms of an Michelson can be measured. This works because light has a finite speed and it takes the light a time t to travel a distance. If there is a difference of distance between the two arms in the Michelson interferometer, one beam will have originated from the light source at an earlier time than the other. By scanning(increasing or decreasing) the wavelength of the light source by changing the current, light at time $t = 0$ and light at time $t = t_1$ will have slightly different wavelength/frequency. When two beams of slightly different frequency are mixed, a beat signal arises. The beat signal has a frequency which is proportional to the difference in distance between the two arms in the interferometer. This technique is called the optical Frequency Modulated Continuous Wave (FMCW) interferometry, and is capable of measuring absolute distances. In addition to this, it is also possible to use this setup to find the velocity of the object with some range finding techniques. This is done by utilizing the Doppler shift, which is a change in frequency because of a deviation in velocity between the observer and the source. Only utilizing the Doppler shift to monitor a structure can measure the vibration frequency, but not monitor slow changes over time, like movement due to temperature changes over several hours. The absolute distance is also of interest to obtain for the focus of a camera system, to find the distance the field of view covers, which can be used to estimate the movement of objects tracked by the camera. To be able to measure the distance of approximately 30 meters with a high accuracy, and to be able to detect a small vibration of this distance, a

laser is suitable. The pulse method could be used, but it would be difficult to achieve a high enough sensitivity. A length difference of 0.1 mm will result in a time difference of 0.6667 ps when light travels back and forth. Instead of developing high-speed electronics to detect small distance changes, frequency modulation can be utilised to detect a beat signal. This thesis will build a prototype based on the optical FMCW technique, and combine this with the Doppler shift to both have a high sensitivity to oscillations(sub mm) and to have the possibility of measuring the absolute distance within some cm.

Chapter 2

Theory

2.1 Optical Frequency Modulated Continuous Wave (FMCW) interferometry

2.1.1 The principle

Introduction

The Frequency Modulated Continuous Wave (FMCW) distance measuring technique has been known for many decades, and has been used in Radars since the second world war [9]. Optical FMCW is based on scanning the frequency/wavelength of the laser, in addition to comparing two different beams to measure the difference in frequency which is called a beat signal. A portion of the laser light is separated from the path towards the object, and directed towards a detector. This beam is called the reference beam. The rest of the laser light, called the object beam, reflects from the object and(after a detour reflecting in a beamsplitter, a second mirror and finally transmitting through the beamsplitter, this is explained in detail next) is added to the same path as the reference beam, overlapping the laser light hitting the sensor. A Michelson interferometer setup, as shown in figure 2.1,

is used to superposition the object and reference beam. Note that other interferometric setups can also be used to perform Optical FMCW, such as the Mach-Zehnder and Fabry-Perot [10, p. 118-119].
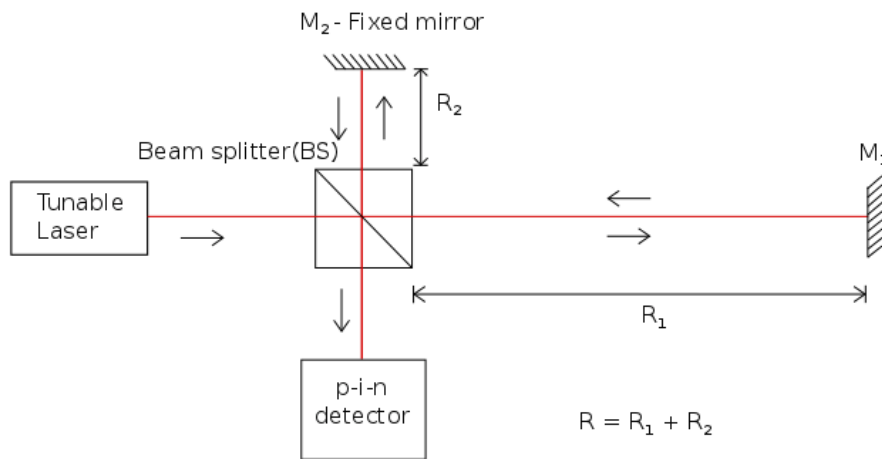
Figure 2.1: A setup for performing optical FMCW distance measurements. The mirror M_1 is placed at the distance which is to be measured, while M_2 is fixed. The two beams overlap at the p-i-n detector, creating a beat signal. This beat signal makes it possible to measure the distance.

Superposition of two electric fields

Assuming all the electric fields are polarized identically, if the two coherent beams overlapping at the sensor have a slight difference in their optical frequency, the intensity will be a sum of both two DC components which originate from each electric field, and an alternating component which has the frequency of the difference between the two electric fields. In equations 2.2 and 2.3 E_{tot} represents the total electric field. If R is defined as the object path length R = (R_1 + R_2), then E_1 represents the reflected electric field that has travelled the path 2R and E_2 represents the reference electric field, which is directly reflected to the detector without travelling the path 2R. ω_2 is the angular frequency of the reference, ω_1 is the angular frequency of the reflection, and ω_{if} is the intermediate angular frequency between the two

electric fields. The same naming convention is used for the phases of the two fields, except that the difference between the two fields is represented by $\Delta\phi$.

The following equations are presented in [10, p. 17-19]. First the relationship between the electric field and intensity is defined as:

$$I = |E(\tau, t)|^2 \tag{2.1}$$

$$
\begin{aligned}
E_{\text{tot}}(t) &= E_1(t) + E_2(t) \\
E_{\text{tot}}(t) &= E_{01}e^{-j[\omega_1 t + \phi_1]} + E_{02}e^{-j[\omega_2 t + \phi_2]} \\
E_{\text{tot}}(t) &= E_{01}e^{-j[(\omega_2 + \omega_{if})t + \phi_1]} + E_{02}e^{-j[\omega_2 t + \phi_2]}
\end{aligned}
\tag{2.2}
$$

$$
\begin{aligned}
I_{\text{tot}} &= |E_{\text{tot}}|^2 = E_{\text{tot}} \cdot E_{\text{tot}}^* \\
I_{\text{tot}} &= (E_{01}e^{-j[(\omega_2 + \omega_{if})t + \phi_1]} + E_{02}e^{-j[\omega_2 t + \phi_2]}) \cdot \\
&\quad (E_{01}e^{j[(\omega_2 + \omega_{if})t + \phi_1]} + E_{02}e^{j[\omega_2 t + \phi_2]})
\end{aligned}
\tag{2.3}
$$

Because in this case $E_{02} \cdot E_{01}^* = E_{01} \cdot E_{02}^*$, equation 2.3 becomes simplified to equation 2.4.

$$
\begin{aligned}
I_{\text{tot}} &= |E_{01}|^2 + |E_{02}|^2 + |E_{01}||E_{02}|[e^{j[\omega_{if}t + \Delta\phi]} + e^{-j[\omega_{if}t + \Delta\phi]}] \\
I_{\text{tot}} &= |E_{01}|^2 + |E_{02}|^2 + 2|E_{01}||E_{02}|\cos(\omega_{if}t + \Delta\phi)
\end{aligned}
\tag{2.4}
$$

The last term in equation 2.3 is the signal that is used in FMCW to measure distances. To create the difference ω_{if} the laser has to be modulated. The modulation can for example be done by driving the laser with a sawtooth current. The difference in frequency between E_1 and E_2 is illustrated in figure 2.3.

Unfortunately the two beams are not perfectly temporally coherent in the real world. All lasers will have some spectral width, and therefore a finite coherence length [11, p. 38]. So if two superposed electric fields originating from the same coherent source are separated in time (or have traveled two different distances), the result will become more complicated than described in equations 2.2 to 2.4. The superimposed fields are now partially coherent, and the phase difference between them will not be constant over time. The interference will therefor be reduced as the path difference between the two arms is increased, until it vanishes when the path difference exceeds the coherence length of the light source. As described in [12, p. 419-420], the statistical properties have to be included in equation 2.4, as shown in equation 2.5.

$$I_{\mathrm{tot}} = |E_{01}|^2 + |E_{02}|^2 + 2|E_{01}||E_{02}||g_{01,02}|\cos(\phi) \tag{2.5}$$

Here ϕ is the argument of $g_{01,02}$, which is the same as described in equation 2.4: $\omega_{if}t + \Delta\phi$ for coherent light. $g_{01,02}$, which is the degree of coherence, is defined as:

$$g_{01,02} = \frac{\langle E_{01}^* E_{02} \rangle}{\sqrt{I_{01}I_{02}}}. \tag{2.6}$$

The visibility of the interference is given by [12, p. 420]:

$$\mathcal{V} = \frac{2\sqrt{I_{01}I_{02}}}{I_{01} + I_{02}}|g_{01,02}|, \tag{2.7}$$

and it is clear that the visibility of the interference is directly proportional to $g_{01,02}$. So if $g_{01,02}=0$, the FMCW will have not produce a beat signal. The reason why the interference, and therefore the beat signal, only appears when the beams are coherent is illustrated in figure 2.2. The mixing of two partially coherent waves can be viewed as two sinusoidal wave trains. If they originated from the same light source, but one is delayed in time in regard to the other,

they will be partially coherent. In figure 2.2 a colour represent the part of the signal that is coherent, with the difference between these parts being a random phase shift. Because detecting intensity is an average of the signal over time, the mixing of the two beams will only produce interference for the coherent parts of the plot [11, p. 38-39], as the mixing of two incoherent beams will only produce random signals which are detected as noise.
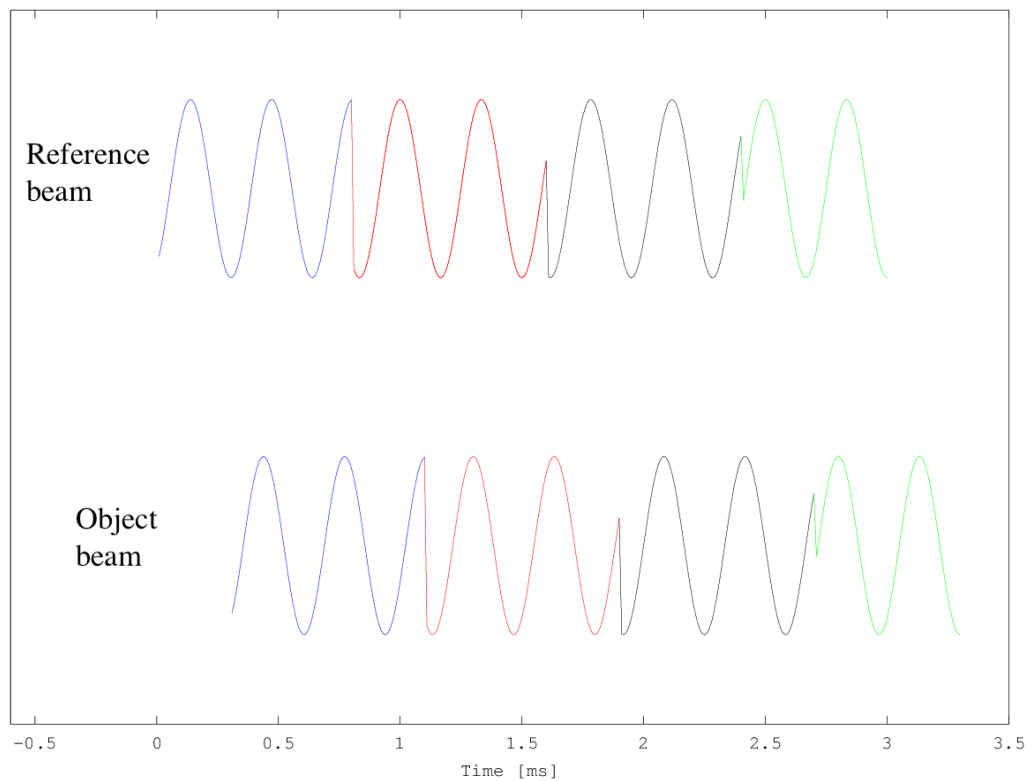
Figure 2.2: A plot of two sinusoidal wave trains that are partially temporally coherent. They have originated from the same light source, but one is delayed by 0.3 ms in regard to the other. The different colours represent the part of the signal that is coherent, with the difference between these parts being a random phase shift. Because detecting intensity is an average of the signal over time, the mixing of the two beams will only produce interference for the coherent parts of the plot [11, p. 38-39].
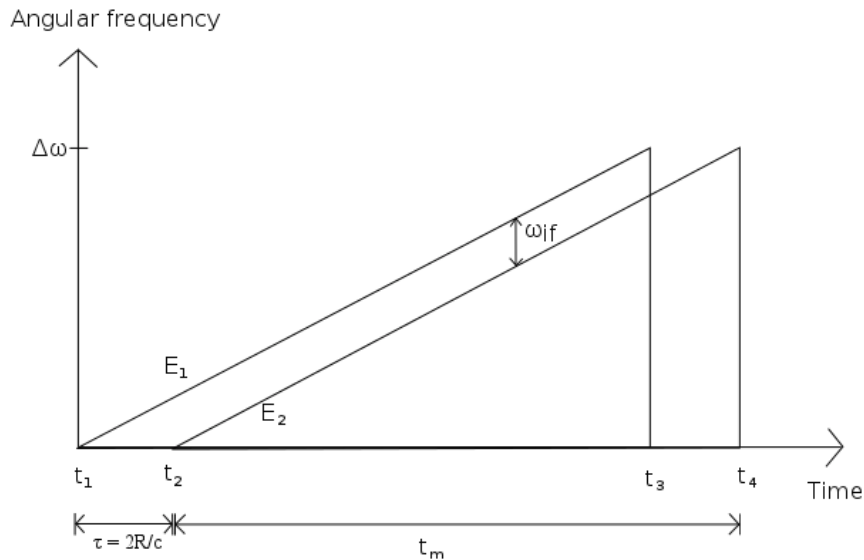
Figure 2.3: A plot of the frequencies the two electric fields will have because of the modulation, as a function of time. In this case the modulation is either saw-tooth or the rising flank of a triangular waveform. E_1 represents the reference beam, which has traveled the shortest path from the light source. E_2(the object beam) originated at the same source at an earlier time, and has therefore a lower angular frequency.

The distance is found by detecting the frequency which the intensity varies with at the detector. This is the beat signal, shown in the last term in equation 2.3. One of the electric fields has been directly reflected from the beamsplitter to the detector, and is therefor the reference signal. The other electric field has traveled a path R_1 to a mirror M_1 and back, and, via the beamsplitter, the path R_2 before it was reflected by mirror M_2 and traveled back through the beamsplitter. It has therefore travelled the object path length $R = R_1 + R_2$ two times. Given that c is the speed of light in air, to travel the distance 2 R takes light the time τ:

$$\tau = \frac{2R}{c}. \tag{2.8}$$

Equations 2.8, 2.9 and 2.10 are presented in [10, p. 17-19]. During the time τ, the laser has been tuned to a different wavelength, changing the frequency of the electric field. The amount of change is determined by the slope of the modulation shown in figure 2.3, which in turn is determined by the period of the modulation signal(t_m) and the amplitude of the scan(Δf). When the two electric fields meet at the p-i-n detector, one was created at the laser a time τ later than the other. Continuing from equation 2.8, the relation between the distance and the shift in frequency is:

$$
\begin{aligned}
\tau &= \frac{2R}{c} \\
\tau &= t_m \frac{\omega_{if}}{\Delta\omega} \\
t_m \frac{\omega_{if}}{\Delta\omega} &= \frac{2R}{c} \\
\omega_{if} &= \frac{2R\Delta\omega}{t_m c} \\
f_{if} &= \frac{2R\Delta f}{t_m c}.
\end{aligned} \tag{2.9}
$$

The final line in equation 2.9 gives the relation between the intermediate frequency(f_{if}) that is measured and that distance the laser light has travelled, in agreement with [4]. This frequency can be measured by performing a Fast Fourier Transform(FFT) of the signal. Equation 2.10 shows how to find the object path length R when the intermediate frequency f_{if} has been obtained.

$$R = \frac{f_{if} t_m c}{2\Delta f} \tag{2.10}$$

2.2 Modulation Waveforms

2.2.1 Sawtooth

The sawtooth modulation consists of a linear increasing(or decreasing) flank, followed by a step to the starting point. This can be seen in figure 2.4. The Fourier series of this waveform is infinite, and the n'th term has an amplitude that decreases by $1/n$. The Fourier series for a sawtooth waveform is given in equation 2.11.
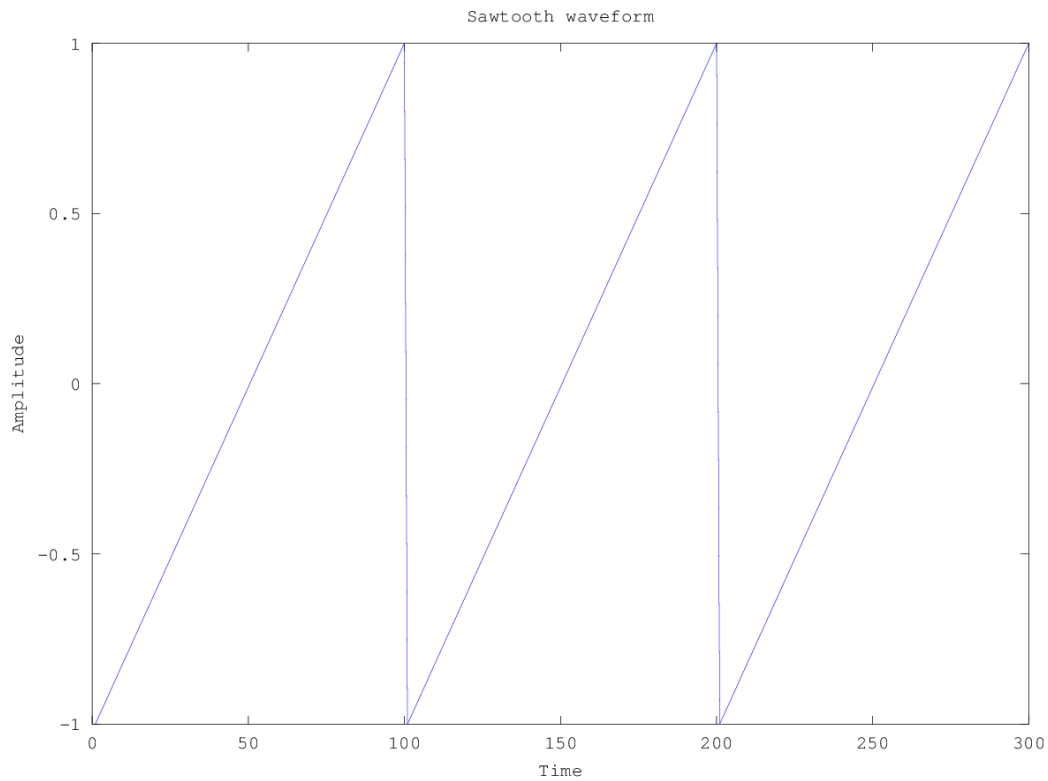
Figure 2.4: A plot showing three periods of the sawtooth waveform.

$$x = \sum_{n=1}^{\infty} \frac{2}{n}(-1)^{n+1}\sin(nx) \tag{2.11}$$

2.2.2 Triangular

A triangular waveform is shown in figure 2.5. The Fourier series for the triangular waveform is presented in equation 2.12, and will, like the Fourier transform of the sawtooth, be infinite in the frequency domain. When comparing this equation to the Fourier series for the sawtooth waveform, equation 2.11, one can see that the terms in the triangular waveform will reduce in amplitude with a dependence of $\frac{1}{n^2}$, compared to the $\frac{1}{n}$ dependence of the sawtooth waveform.

$$x = \frac{4}{\pi} \sum_{n=0}^{\infty} \frac{\cos(2n+1)x}{(2n+1)^2} \tag{2.12}$$
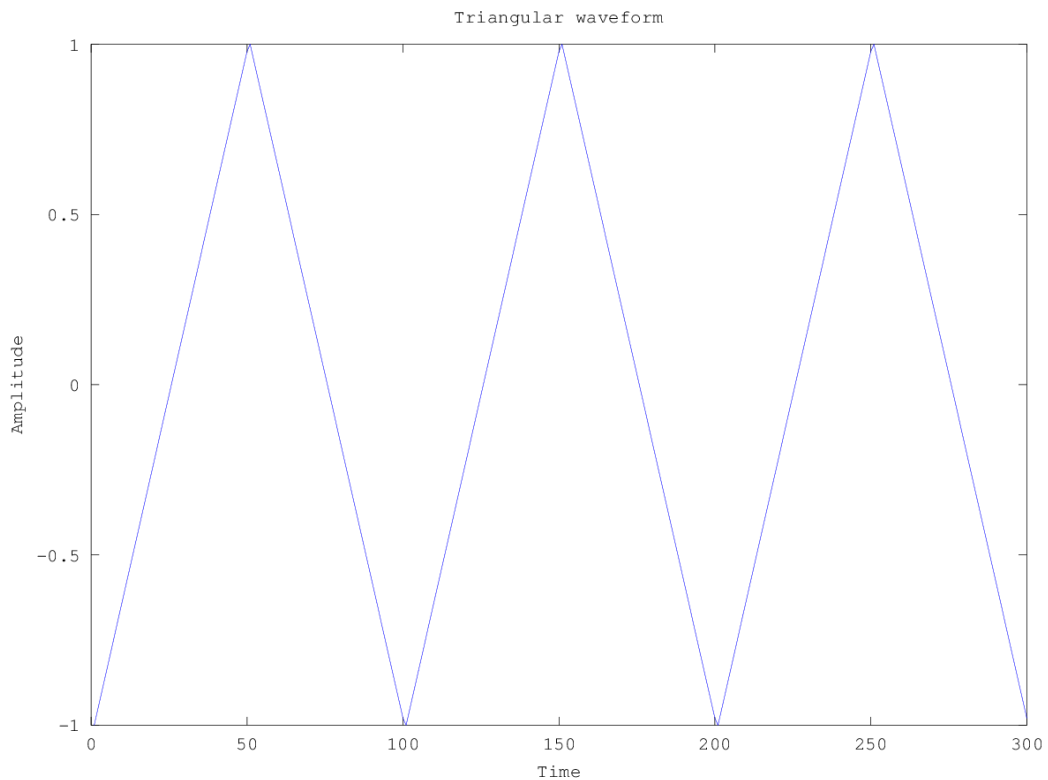
Figure 2.5: A plot showing three periods of the triangular waveform.

2.2.3   Sinusoidal

It is also possible to modulate the frequency sinusoidally, which will produce a intermediate frequency which is periodically as a sine function. This can be seen in figure 2.6. Since the sine waveform has a continuous derivative, the frequency of the produced beat signal will also be continuous. There will therefore not be any undefined time slots, as is the case in the time τ after the discontinuity in the derivative of the sawtooth and triangular modulation. The sinusoidal modulation can also detect the Doppler shift of the intermediate frequency, as can the triangular modulation. This is because of both a rising and falling flank being part of the modulation, while the Doppler shift is only an upshift or downshift for movement in one direction. One advantage sinusoidal modulation of a laser has over the sawtooth and triangular modulation is that supplying a sinusoidal alternating current will modulate the wavelength of the laser as a sine [13]. This is not the case for the other two, which require a compensated waveform for the wavelength tuning to have a linear waveform. There are some difficulties with this technique also, as when the intermediate frequency approaches zero, the accuracy of the measurement will go down [10, p. 34]. This method of modulation will not be used in this project.
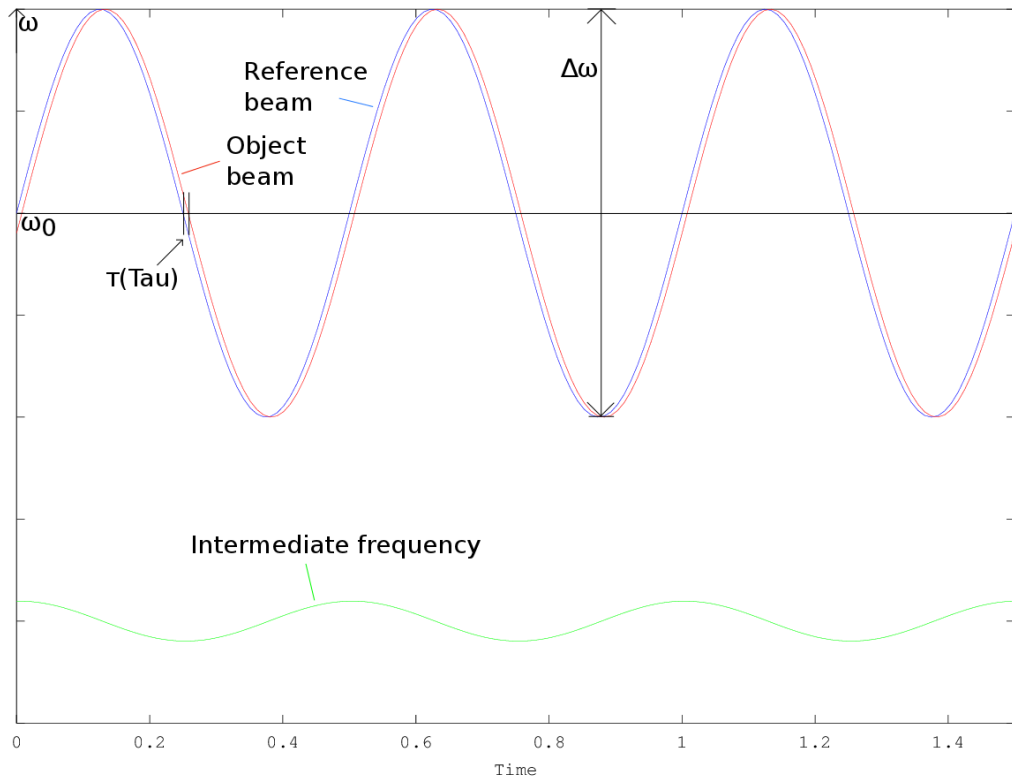
Figure 2.6: A plot showing how a sinusoidal modulation will create an intermediate frequency in the FMCW setup, as showed in [10, p. 34]. The object beam(red) and reference beam(blue) are slightly separated in the sine modulation the their angular frequency, creating a varying intermediate (angular) frequency(green).

2.3 Doppler shift

The reflected EM-wave changes frequency if the object it is reflected from has a velocity towards or away from the observer. This phenomena is called the Doppler shift. The change of frequency will also arise if the observer moves, but here the equation will be given for a stationary observer. The equations here are found in [14]. As seen in figure 2.7, when the first wavefront reaches the object, the next wavefront is the distance λ away from the object.
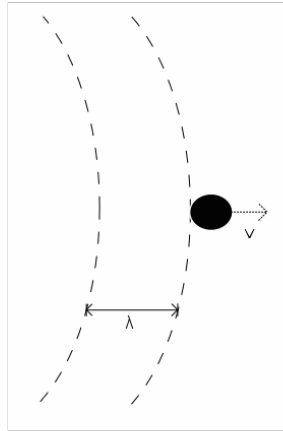
Figure 2.7: A simple plot showing that velocity of an object will give rise to the Doppler shift. The position of an object is shown as the first EM-wave strikes the object. At this point of time the distance from the object to the next wavefront of the EM-wave is λ. During the time it takes the next wavefront to reach the object, the object itself will have moved a small distance away from this position. Viewing the object as a new source of EM-waves as it reflects these wavefronts, the distance between the two reflected wavefronts will be longer than λ, equivalent to an EM-wave with a longer λ.

The time t_1 the first wavefront uses to reach the object is:

$$t_1 = t_0 + \frac{2R_0}{c - v}. \tag{2.13}$$

Here R_0 is the distance the object had from the observer at the time the EM-wave left the observer. t_0 is the time the first wavefront left the observer, c is the speed of light in air, and v is the velocity of the object away from the observer. The time t_2 the second wavefront uses to reach the object is:

$$t_2 = t_0 + T + \frac{2R_1}{c - v}, \tag{2.14}$$

where T is the period of the EM-wave. Subtracting equation 2.13 from 2.14 gives the time difference Δt:

$$t_2 - t_1 = t_0 + \mathrm{T} + \frac{2R_1}{\mathrm{c} - v} - t_0 - \frac{2R_0}{\mathrm{c} - v}$$

$$\Delta t = \mathrm{T} + \frac{2R_1 - 2R_0}{\mathrm{c} - v}. \tag{2.15}$$

Since R_1 and R_0 have the relation $R_1 = R_0 + v\mathrm{T}$, equation 2.15 becomes:

$$\Delta t = \mathrm{T} + \frac{2v\mathrm{T} + 2R_0 - 2R_0}{\mathrm{c} - v}$$

$$\Delta t = \mathrm{T} + \frac{2v\mathrm{T}}{\mathrm{c} - v}$$

$$\Delta t = \mathrm{T}\frac{\mathrm{c} + v}{\mathrm{c} - v}. \tag{2.16}$$

This is the period of the reflected signal, which is the time between the wavefronts that the observer will see. The received frequency f_R becomes:

$$f_R = \frac{1}{\Delta t} = \frac{\mathrm{c} - v}{\mathrm{T}(\mathrm{c} + v)}$$

$$f_R = f_0 \frac{\mathrm{c} - v}{\mathrm{c} + v}. \tag{2.17}$$

When the velocity of the wave is much larger than the velocity of the object, the following approximation can be made:

$$\frac{1}{1 + v/c} = 1 - \frac{v}{c} + \frac{v^2}{c^2} - \dots \tag{2.18}$$

When inserting this into equation 2.17, the equation becomes:

$$f_R = f_0(1 - \frac{v}{c})(1 - \frac{v}{c} + \frac{v^2}{c^2} - ...)$$

$$= f_0(1 - \frac{2v}{c} + ...) \approx f_0(1 - \frac{2v}{c}) \qquad (2.19)$$

$$f_R \approx f_0 - \frac{2v}{c/f_0} = f_0 - \frac{2v}{\lambda}.$$

And finally this becomes the Doppler shift:

$$f_D = f_R - f_0 \approx -\frac{2v}{\lambda}. \qquad (2.20)$$

f_D is the Doppler shift which will be the frequency of the beat signal if two beams with frequency f_R and f_0 are mixed together.

2.4   Laser Doppler Vibrometer

Laser Doppler Vibrometry (LDV) is a method for measuring vibration that is based on the Doppler effect. This method cannot measure the absolute distance, but measures the frequency shift by detecting a beat frequency in an interferometric setup. In a heterodyne regime one arm is frequency shifted, so that a Doppler shift will result in a change of the beat frequency. The homodyne regime will not be treated here and in the rest of the text the heterodyne regime will be presumed. Unlike the optical FMCW setup, the laser in a LDV is not modulated in wavelength. When the beams from the two arms are mixed, a beat frequency arises and any change to this beat frequency will be caused by the Doppler shift in the measurement arm. The equations for the intensity illuminating the detector will be similar to equations 2.4 and 2.5. A possible setup can be seen in figure 2.8, and is in this reference called an intermediate heterodyne frequency system. In figure 2.8 the frequency shift is done by utilizing a Bragg cell, which is an acousto-optic modulator that will diffract some parts of the light, and transmit the rest [12, p. 806]. It is also

possible to build a self-mixing system for heterodyne LDV measurement [15].
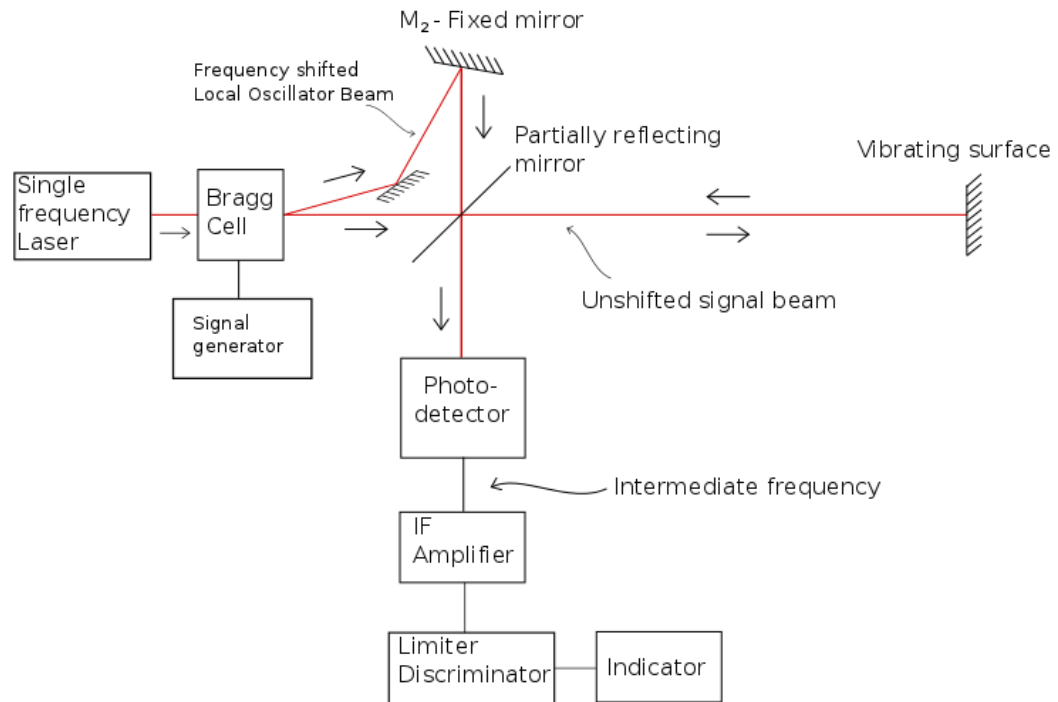
Figure 2.8: A block diagram showing a possible setup of a Laser Doppler Vibrometer, as described by [16, p. 4]

2.5   Detection method

As described in [10, p. 225-230] it is possible to detect the beat signal with several different techniques. The beat frequency is the signal that hold the information about the distance, and a simple way to find the frequency is to measure the time between two consecutive peaks or zero crossings using an oscilloscope. But for automated measuring some other techniques are pratical:

Frequency counting

One simple way to measure the frequency of the beat signal is to use an operational amplifier, an amplification limiter and a frequency counter [4]. This system will count the peaks of the beat signal. The resolution of this technique will depend on the modulation frequency, the scan Δf of the laser source, the measurement distance, as well as highest frequency the detector can measure. I.e. if the modulation frequency is set to 1 kHz sawtooth waveform, the laser source is scanned over 50 GHz and the measurement is performed at a distance of 10 m, the resulting beat frequency will be given by equation 2.9 as: $f_{if} = \frac{2 \cdot 10 \cdot 50 \cdot 10^9}{1 \cdot 10^{-3} \cdot 3 \cdot 10^8} = 3.33$ MHz. Given that the sample will be done during almost the whole period of the modulation wave, if the time $\tau = \frac{2 \cdot 10}{3 \cdot 10^8} = 66.7$ ns is neglected, the sample will be of $1/1000$ of $3.33 \cdot 10^6$ periods. This results in $3.33 \cdot 10^3$ positive peaks, or $6.67 \cdot 10^3$ peaks is both positive and negative maximas are counted. If counting only positive maximas, a difference of 1 peak will result in a change in distance of 3 mm. Because the phase of the signal might make the frequency counting just exclude or include a peak, there will be some uncertainty. This method is known as time-fixed cycle counting, while another method is called number-fixed cycle counting. This method measured the time between the first peak and the n'th peak, where n is the static number set in advance. This will improve on the uncertainty because the system will no longer divide the number of peaks by the static value of 1 ms, but instead adapt this to the time of the actual measurement. For low frequency beat signals, none of these are accurate, but for this case the Pulse-filling method can be used. This method measures the period of the beat signal by counting the peaks of a high frequency signal within one period of the beat signal.

2.6 Noise

In any detector system noise will be present. The noise can be separated into three main categories: *Shot noise*, *1/f noise* and *Thermal noise*. The

equations presented here were found in [12, p. 777-786] and [17, p. 131-136].

2.6.1   Shot noise

Shot noise, also known as photon noise or quantum noise if the random arrival of charges can be modelled as poisson distributed, arise from the discrete nature of electrons. All components containing a pn-junction produce shot noise. Equation 2.6.1 shows how the shot noise increases as the square root of the signal. This means that the signal increases faster than the shot noise, and the SNR therefore increases with the signal.

$$\langle i_{\mathrm{N}} \rangle = \sqrt{2ei} \ \mathrm{A/Hz}^{1/2}. \tag{2.21}$$

Here $\langle i_{\mathrm{N}} \rangle$ is the spectral density of the shot noise of the photocurrent, e is the charge of an electron, and i is the photocurrent. All detectors also have a dark current, which when added to the current in equation 2.6.1 become:

$$\langle i_{\mathrm{N}} \rangle = \sqrt{2e(i + i_d)} \ \mathrm{A/Hz}^{1/2}, \tag{2.22}$$

where i_d represents the dark current. This current emerges from thermally generated carriers [10, p. 96].

2.6.2 $1/f$ noise

$1/f$ noise, also known as flicker noise, is a white noise with a roll-off at higher frequencies, or described as a *pink* noise. This means that it is dominant in the low frequency area. It comes from contaminations around the surfaces of IC connections, fluctuations in charge carriers in carbon, electron migration in conductors and several other sources [17, p. 468]. $1/f$ will only show up

when a current is actually flowing. The rms value of $1/f$ noise is described by equation 2.23:

$$v_{1/f} = iR\sqrt{\frac{A\Delta f}{f}}, \tag{2.23}$$

where A represents a dimensionless constant, i the current flowing through the resistor R, f is the central frequency and Δf is the frequency bandwidth [10, p. 97].

2.6.3 Thermal noise

Thermal noise(also called Nyquist noise or Johnson noise) originates from the random motion of carriers in resistive materials, R in equation 2.6.3, due to thermal effects [12, p. 786]. This is also known as Lattice Generation-Recombination Noise [17]. The thermal noise current is proportional to the square root of the temperature and bandwidth, and inversely proportional to the square root of the resistance R, as can be seen in equation 2.6.3.

$$i_t^2 \approx 4kTB/R \; [\text{A}]^2 \tag{2.24}$$

Where i_t^2 is the square of the thermal noise current,8 T is the temperature of the resistor, B is the bandwidth that is treated and k is Boltzmanns constant.

Chapter 3

Experimental Setup

In this chapter a prototype of the setup for optical FMCW displacement and distance measurements is presented. Two different lasers are tested in the design.

3.1 Equipment

3.1.1 List of equipment

- Laser 1: Oclaro 760 nm single mode VCSEL with peltier element and thermistor in TO510, appendix B. Line width = 20 MHz, which corresponds to a coherence length of 15 m.

- Laser 2: 1565 - 1625 nm, line width (typ) = 2 MHz, which corresponds to a coherence length of 150 m. The Laser was always driven by a DC current of 90 mA, and the modulation was coupled over a resistance of 170 Ohm, resulting in a modulation current of 29.4 mA for a voltage of 5 V pk-pk.

- Lens 1: 1" convex lens, focal length approximately 30 mm. Producer unknown.

- Lens 2: Thorlabs part number LB1723-A, diameter 2" or 50.8 mm convex lens, focal length 60 mm.

- Doublet lens: Melles Griot part number 06LAI003/076. Achromatic, diameter 10 mm, focal length 25 mm, anti-reflective coating for 760 nm.

- Beamsplitter 1: Thorlabs part number BS016, 50:50 Non-polarizing cube, 400-700 nm, 20 mm.

- Beamsplitter 2: Sapphire glass window, 30 mm in diameter, 1 mm thickness, non-wedged, supplied by NEO.

- Detector 1: Newport 818-BB-21 Si-detector, appendix D.

- Detector 2: Fermionics Opto-Technology FD3000W InGaAs PIN Photodiode, appendix E.

- Power meter: Thorlabs PM100D console, SN: P0005536. Photodiode Thor Labs S130VC, SN: 12112303, Wavelength range 200-1100 nm.

- Function generator for modulating the laser: HP 33120A 15 MHz Function/Arbitrary waveform generator, serial number US34000666.

- Function generator for modulating the subwoofer: Iso-Tech synthesized Function Generator GFG 2004, serial number: 907C198G2.

- Laser Gas 2 system from NEO for controlling the laser and detector.

- 12" subwoofer from Biltema, connected to a custom amplifier which made it possible to oscillate the speaker at frequencies down to 0.5 Hz using an external signal generator.

3.1.2 Characterisation of Laser 1 Oclara 760 nm VCSEL

A characterisation was done for Laser 1: Oclara 760nm VCSEL by focusing the laser light into a fiber connected to an optical spectrum analyzer. Cou-

pling a laser into a fiber is not trivial, but the coupled intensity needed for exceeding the noise level in the optical spectrum analyzer is not high. A SNR level of about 40 dBm was achieved with only 25 μW of intensity at the end of the fiber. According to the data sheet of the optical spectrum analyzer, this instrument had a resolution of 0.06 nm. This is a rather low resolution compared to other spectrum analysers, but for finding the centre wave length of Laser 1 the result is sufficient to indicate how much the laser is scanned. The spectrum for Laser 1 driven by a DC current of 8 mA is plotted in figure 3.1. Note the second peak just above 760 nm. This peak is about 11.7 dBm lower in amplitude than the main peak. A total of 81 spectrums were captured, with the laser supplied with 4.77-8.00 mA of current. Each of the measurements were averaged over 20 measurements, and 1001 sample points were stored over a interval of 3 nm. The centre wavelength for each measurement was found with a centre of mass calculation, and is presented in figure 3.2. As mentioned, the second peak was 11.7 dBm weaker than the main peak, meaning that this peak does not significantly affect the centre of gravity. The measurements were done to characterise Laser 1, and to find the scan of the laser relative to the current supplied to it. However, this result did not match with measurements done with Laser 1 in the lab. The reason for this is that the faster the currents feed to the laser, the less the laser is scanned. This is covered by [13, p. 3 or 174]. Even worse is that the nonlinear characteristic of the scan is also dependent on the modulation frequency and over how many nm/GHz the scan is. This is mainly because of thermal fluctuations [18, p. 3]. A static measurement like this will therefore not provide information that can be used to create a compensated waveform for linearising the scan. A lot of time was wasted on getting a somewhat obsolete spectrum analyser to work, and both getting the measurements done and interpreting them.
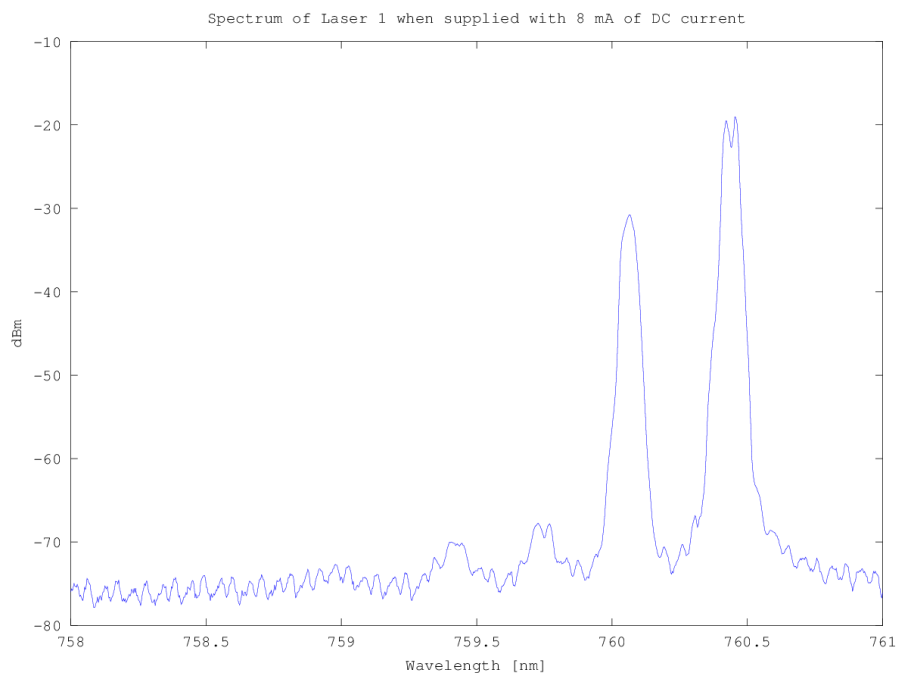
Figure 3.1: A logarithmic plot of the spectrum of laser 1 when supplied with a current of 8 mA. A second peak is clearly visible when supplying the laser with this current.
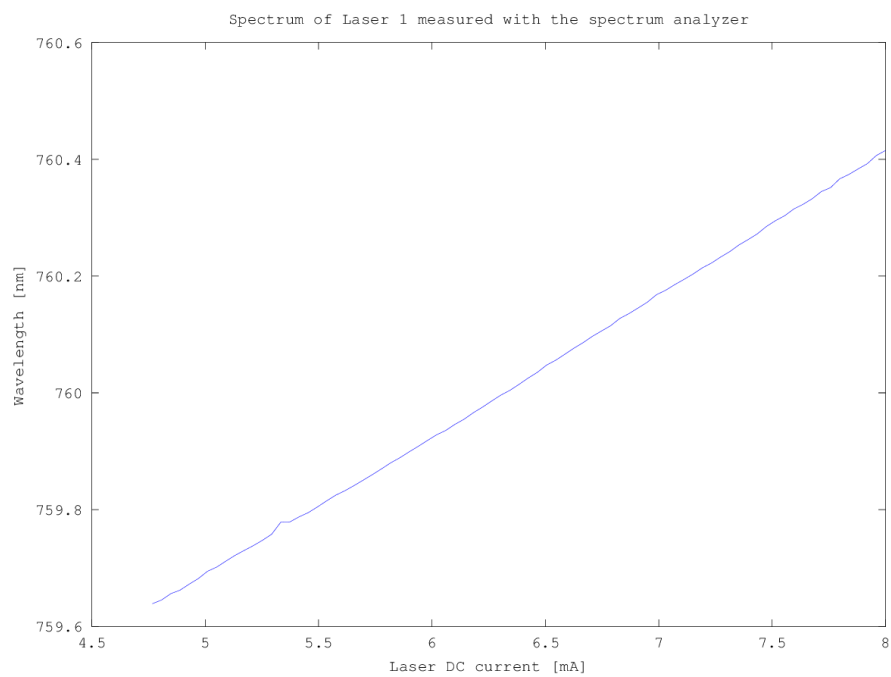
Figure 3.2: A plot of the centre wavelength scanned by supplying Laser 1 with a DC-current of between 4.77-8 mA. From the figure, it is clear that the scan is close to linear. The measurement was done to characterise Laser 1, and to find the total scan of the laser.

It is also possible to use a Fabry-Pérot etalon, to measure how much the wavelength of the laser is scanned. It is based on the principle that two partially reflecting surfaces placed parallel to each other will exhibit a transmittance and reflectance that is wavelength dependent, due to constructive and destructive interference [17, p. 37]. The Fabry-Pérot etalon will create interference and transmit peak intensity periodically when the scan passes the bandwidth of the etalon. I.e. if a Fabry-Pérot etalon with a bandwidth of 1 GHz is used and 50 peaks are observed over one scan, then the frequency of the laser light has been scanned over 50 GHz. By finding the time period between these peaks, the nonlinearity of the scan could be approximated, and perhaps corrected to some degree.

The ratio between maximum and minimum reflectance of a Fabry-Pérot etalon will depend on the finesse of the etalon, as seen in equation 3.1 [17].

$$T_{F-P} = \frac{1}{1 + \frac{4R}{(1-R)^2}\sin^2(nk_0 d\cos\theta)}, \tag{3.1}$$

where R is the reflectance of the surfaces, d is the spacing between them, n is the refractive index of the material and k_0 is the wavenumber.

3.1.3 Characterising the retroreflectors

By measuring the intensity of the beam before and after it was reflected in the retroreflectors, the reflectance value could be established. The measured value was between 68-72 % for the two retroreflectors. This is also presented in table 3.1, where both the loss/reflectance in the lenses and BS also are presented. The reflective layer on the retroreflectors are of metal. These components are best suited for visible light and have higher losses for IR light. Laser 1 which has a wavelength of 760 nm, was used to test the reflectance of the retroreflectors. This test showed a high loss compared to the expected reflectance of the mirrors, even though the beam reflects in 3 mirrors in a retroreflector before travelling back in parallel to the direction it

originated from. The low reflectance might come from both the component being optimal for other wavelengths than Laser 1, and it might be because of damage/scratches or dirt on the surface of the mirrors.

3.1.4 Characterising the beamsplitter

There are several types of BS available, both polarizing and non-polarizing, and of different values of reflection and transmittance. If a polarizing BS is used the beam that is transmitted and the beam that is reflected will be orthogonally polarized to each other. The object beam will then hit the mirror at the object and return to the BS. But since the beam is still linearly polarized at the polarization that is (ideally) 100% transmitted and 0 % reflected in the BS, non of the light will be reflected to mix with the reference beam. The object beam will instead end up in a beam stop like in figure 3.4, or be back reflected into the laser(or optical isolator if present) like in figure 3.3 depending on the alignment and the type of mirror used at the object. Therefore a non-polarizing BS must be used, and the ideal reflectance value is 50:50, as described in subsection 3.2.1, with as little absorption as possible. The reflectance and transmittance of BS 1 was measured by focusing the reflected and transmitted beam into the power meter. For this test, Laser 1 was driven by a DC current of 6 mA.

Component configuration	Intensity[mW]
Directly from laser	0.76
Lens 1 and 2	0.61
Lens 1, transmitted in BS 1, and lens 2	0.22
Lens 1, reflected by BS 1, and lens 2	0.36
Lens 1, reflected by retroreflector 1, and lens 2	0.44
Lens 1, reflected by retroreflector 2, and lens 2	0.42

Table 3.1: Transmission and reflectance of BS 1, the lenses and the retrore-flectors.

From the measured values presented in table 3.1, it is clear that the lenses introduce loss in the beam path. This is probably because they are best suited for the wavelength interval of 400-700 nm, and that they have some scratches and dirt on the surface. The reflectance and transmittance of the 50:50 BS 1 are not equal, which might come from the wavelength of Laser 1 being just outside the wavelength interval of BS 1. The approximated values are then R = 59% and T = 36%, with an absorption of about 5%. In later tests done with Laser 2, which has a wavelength at 1565-1625 nm, BS 1 absorbed too much to achieve the beat signal at even the short distance of 30-40 cm. BS 1 was therefore swapped with BS 2 which is the sapphire glass set at 45 degree angle to the beam path. This resulted in approximately 10% reflection, which is far from ideal, as will be covered in subsection 3.2.1. The reason for this choice was because of a limited selection of parts that were available in the lab and at NEO.

3.2   Practical setup

The setup in figure 2.1 is a simplified version of a possible final setup. Feedback reflected back into the laser can cause noise, reduce coherence length, and damage the laser. It might also end with loosing control of the direction and stability of the laser beam. It is advisable to remove this feedback, and this is usually done by inserting a Faraday-isolator. It is also possible to use a cube corner retroreflector to separate the reflected beam but still keeping it in parallel with the incident beam. This solution is used in this prototype, as seen in figure 3.4. The concept of using retroreflectors in this way is well known [10, p. 118]. The beat signal should only be sampled when the signal is valid, which is between time t_2 and t_3 in figure 2.3. At a time delay τ before and after this time slot, the signal is not defined and the result will be noise in this measurement. This process is repeated as the modulation is periodic. A possible future implementation is shown in figure 3.3. Noise can be reduced by applying a trigger, and therefor avoiding the undefined time slot. A trigger from the signal generator can be used to sample the signal
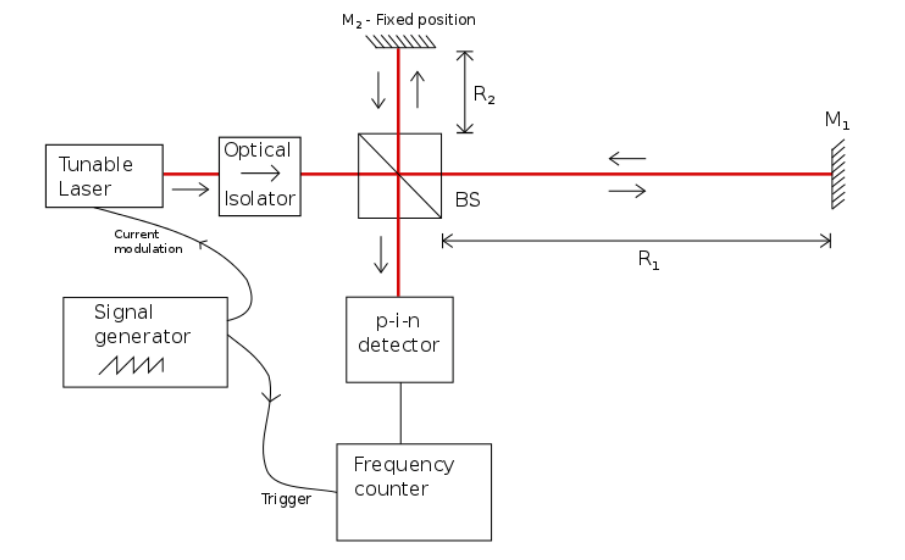
when the beat signal is valid.

Figure 3.3: A possible setup for performing FMCW distance measurements. Using the signal generator to trigger the sampling of the signal can avoid the time slots when the beat signal is undefined. Also note the optical isolator, which is important to avoid back-reflection into the laser.
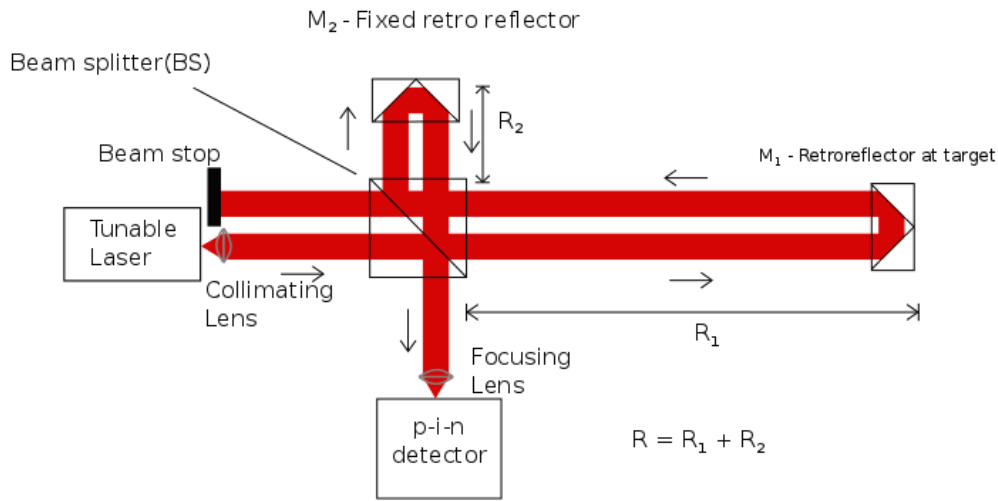
Figure 3.4: The setup of the prototype used to test the concept of FMCW, also illustrated in [10, p. 118]. The figure illustrates how the retroreflectors can be used to separate the initial laser beam from the reflected beam, so that back-reflection into the laser can be avoided without the need for a Faraday isolator. Retroreflectors can also make alignment simpler because they reflect the beam in parallel, possibly shifted, back the direction which the light originated from.

3.2.1 Optimal reflectance of the beamsplitter

The optimal reflectance of the BS is R = 0.5 for maximising the beat signal amplitude. To find this value for the reflectance of the BS it is necessary to see what affects the fields shown in equation 2.4. Specifically the amplitude of the time-varying part of equation 2.4 is of interest, as this is the signal that is measured in FMCW. The electric field E_2 is reflected at the BS and travels directly to the p-i-n detector. The other electric field, E_1, passes through the BS, reflects at mirror M_1, reflects at the BS on the opposite side, reflects at mirror M_2 and passes through the BS before it is superposed with the first electric field. The two electric fields are shown in figure 3.5.
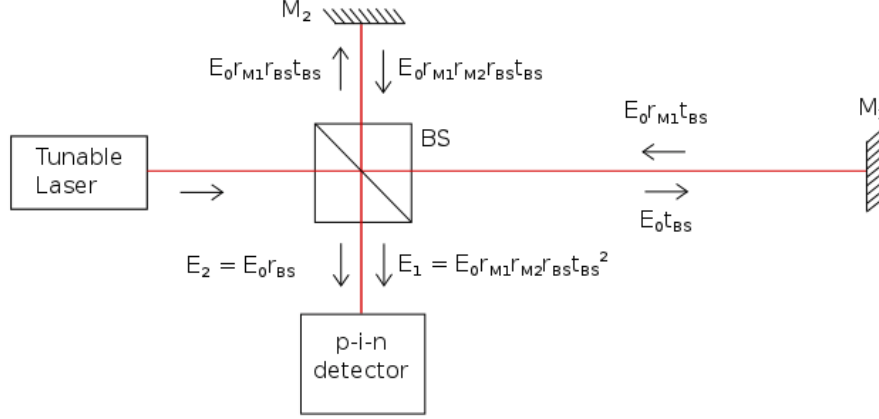
Figure 3.5: A figure showing the electric fields at different stages of the path through the Michelson interferometer setup.

Equation 3.2 shows the value of E_2. The amplitude reflection of the BS is represented by r_{BS}. If a glass window is used as the BS, this variable represents the sum of both the front side and the back side reflection. This is true if the glass has not been treated with an anti-reflective coating or is wedged.

$$E_2 = E_0 r_{\mathrm{BS}} \tag{3.2}$$

The amplitude E_1 is more complicated. The amplitude at different parts of the setup is shown in figure 3.5. Here t_{BS} is the amplitude transmission of the beamsplitter, while the amplitude reflection of mirror M_1 and M_2 are represented by r_{M1} and r_{M2}.

$$E_1 = E_0 r_{\mathrm{M1}} r_{\mathrm{M2}} r_{\mathrm{BS}} t_{\mathrm{BS}}^2 \tag{3.3}$$

To find the optimal reflectance of the beamsplitter to maximize the signals, amplitude E_1 and E_2 can be multiplied together and differentiated with re-

spect to r_{BS}. The differentiated function is then set equal to zero, allowing r_{BS} to be found. The following equations have been derived:

$$
\begin{aligned}
I &= 2E_2 E_1 \\
I &= 2E_0 r_{\mathrm{BS}} E_0 r_{\mathrm{M1}} r_{\mathrm{M2}} r_{\mathrm{BS}} t_{\mathrm{BS}}^2 \\
I &= 2E_0^2 r_{\mathrm{M1}} r_{\mathrm{M2}} r_{\mathrm{BS}}^2 (1 - r_{\mathrm{BS}}^2) \\
I &= 2E_0^2 r_{\mathrm{M1}} r_{\mathrm{M2}} (r_{\mathrm{BS}}^2 - r_{\mathrm{BS}}^4) \\
\frac{dI}{dr_{\mathrm{BS}}} &= 2E_0^2 r_{\mathrm{M1}} r_{\mathrm{M2}} (2r_{\mathrm{BS}} - 4r_{\mathrm{BS}}^3) = 0 \\
0 &= 2r_{\mathrm{BS}} - 4r_{\mathrm{BS}}^3 \\
0 &= 1 - 2r_{\mathrm{BS}}^2 \\
r_{\mathrm{BS}} &= \frac{1}{\sqrt{2}}
\end{aligned}
\tag{3.4}
$$

The solution to the last line in equation 3.4 gives the optimal amplitude reflectance for the beamsplitter when seeking to maximise the term $|E_1||E_2|$ from equation 2.4. The total reflectance of the BS is the square of the amplitude reflectance, $R = r^2$, which results in the total reflectance of the BS of $R = 0.5$ to be the optimal reflectance. This is also shown in the plot in figure 3.6.

With BS 2, the reflected intensity was 76 μ W when the incidental intensity was approximately 0.76 mW. This equals about 10 % reflection in intensity from the sum of both front side and back side reflection. With a cube BS inserted instead, the reflected intensity was 0.28 mW. This corresponds to approximately 35 % reflectance. The transmission was approximately 0.192 mW with the BS inserted. This indicates a large loss in the BS which has to be accounted for in the equations if no BS with approximately 0% loss can be found among optical producers for the required wavelength.
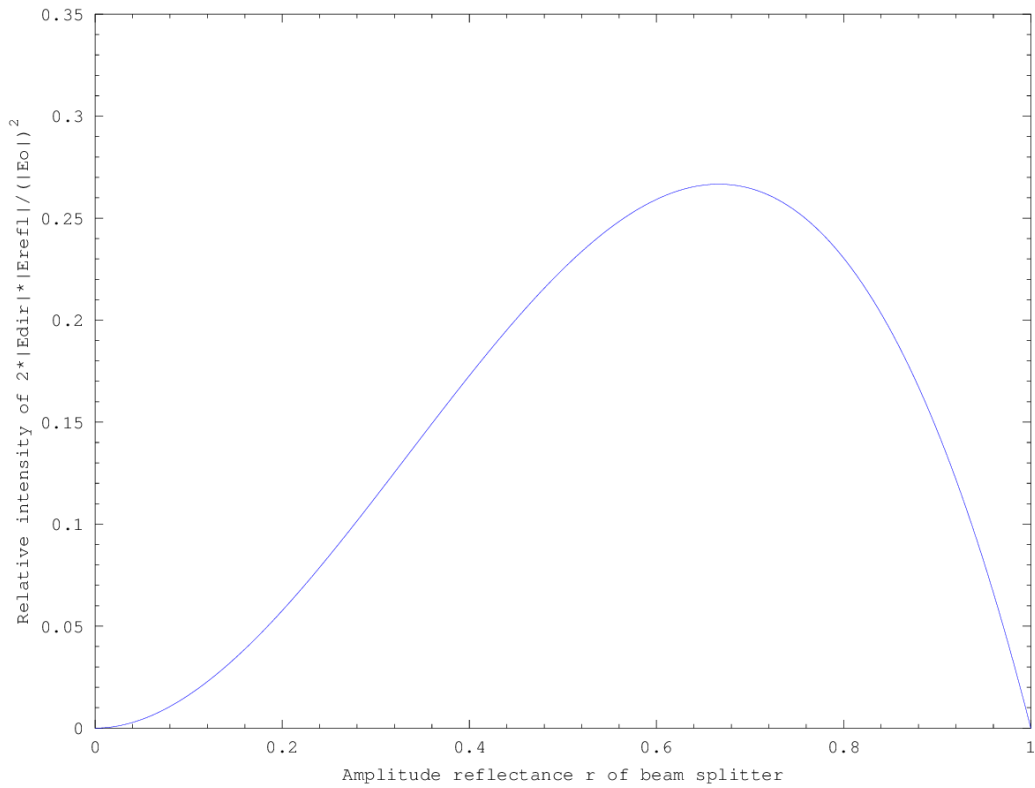
Figure 3.6: A plot showing the intensity of the signal for different reflectance values for the beamsplitter. The reflectance of the mirrors has been set to $r_{M1}r_{M2} = 0.9$. This is a guess, as the reflection of mirrors can be higher, but in this case, with older retroreflectors, some damage/scratches and dust, and a laser with a NIR-wavelength, the reflection was lower.

3.3 Coherence length

As noted in section 2.1.1 the coherence length of the light source is crucial for interferometry. In [19] a low cost light source is examined to try to design a Doppler Lidar system. The path difference between the two arms of an interferometer is where the coherence length is the limitation to achieve interference. In the balance scheme, the arms are approximately the same length, but in an unbalanced scheme, this is not the case. Even though the setups described here are unbalanced, the difference between the two arms could be lowered, so that the requirements of the laser would be lowered.

This would mean that the line width of the laser(inversely proportional to the coherence length) could be wider, making the laser cheaper. The reference arm can for example be extended by using multiple mirrors or by coupling the light into a fiber, which is a part of the Mach-Zehnder interferometer in [19]. Coupling into a fiber would be possible in a setup like the one illustrated in figure 3.3 if the BS was rotated 90 degrees, and of course the coupling components and the fiber was added. For alignment, the retroreflector setup in figure 3.4 would allow the input to the fiber and the fiber end to be placed a small distance parallel to each other. But it will not be done in this project due to the challenges introduced by coupling into a fiber, and other challenges such as polarization control. It would also increase the complexity and the cost of the system which goes against the objective of this project. Laser 1 has a line width of 20 MHz, which corresponds to a coherence length of 15 m. This should make is possible to measure distances up to 7.5 m, but in the lab the signal was only detectable for distances up to 3 m. There are several possible reasons to why the theoretical 7.5 m was not achieved, like the collimation of the beam and alignment of the components being imperfect. Also, back reflections into the laser might introduce noise which could reduce the coherence length. Laser 2 was therefore introduced. Laser 2 has a line width of 2 MHz, which equals a coherence length of 150 m. The coherence length should therefore not be the limiting factor to achieve a measurement distance of up to 30 m.

3.4 Measurement technique

The measurements were done by mounting the retroreflector representing the target at the membrane of a 12" subwoofer(large speaker). This can be seen in figure 3.7. The subwoofer was connected to a power supply, which again was connected to a frequency generator(the Iso-Tech synthesized Function Generator). This made it possible to oscillate the retroreflector at low frequencies, down to 0.5 Hz, with an amplitude of 0.5 cm(1 cm peak to peak). The tests were performed with a triangular modulation for ease of measure-

ment, at 0.5 Hz. This made it possible to start a stop watch at the beginning of one of the cycles, so that even at a distance of more than 10 m, it was possible to know if the speaker was travelling towards or away from the system. The triangular modulation should also produce a near linear movement of the speaker membrane, translating to a constant velocity until the change in direction every half period. This made the exact time of sampling less important, unlike a sine movement would have. The samples for each distance were taken both for a static object, and with constant movement towards and away from the system. The system was placed on a rolling table, as seen in the image in figure 3.8. The image in figure 3.9 shows a better view of the optical part of the setup. A small change in the setup shown in figure 3.9 as opposed to the figures shown in this chapter and the previous chapter is that the BS has been rotated 90 degrees. The equation for the optical path difference of the object beam and reference beam shown in figure 2.1 is in this case changed to R = R_1 - R_2.

Figure 3.7: An image showing the retroreflector mounted on the 12" subwoofer(speaker), for oscillating the object. The subwoofer was driven with a 0.5 Hz triangular modulation, which resulted in a peak-peak movement of approximately 1 cm, which results in a velocity of 0.01 m/s.

Figure 3.8: An image of the prototype setup placed on a rolling table. In the image the following components are visible, starting from the top left: the Picoscope oscilloscope, an IR-sensor card, a signal generator, power supply for Laser Gas 2, the detector board, in front the optical setup shown in figure 3.9, and in the back the main unit of NEO's Laser Gas 2.
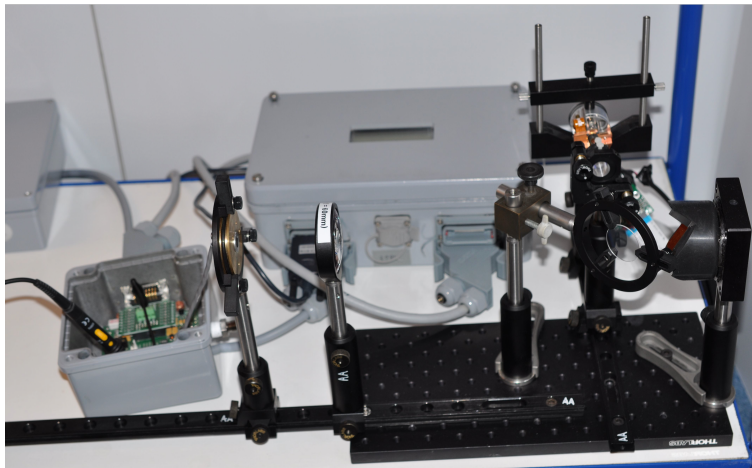

Figure 3.9: An image of the optical part of the prototype setup. To the left is the detector and detector lens, in the middle is the sapphire glass mounted at 45 degrees, behind this is the laser and the doublet lens and to the right is one of the retroreflectors.

Chapter 4

Results

The measurements presented here were produced with Laser 2 in the proto-
type setup, shown in figures 3.7, 3.8 and 3.9. First a raw signal, along with
the filtered signal and the peaks of the beat signal are shown. This is done
for both a static object, and for movement toward and away from the setup,
at a distance of 40 cm. The laser was modulated with a 300 Hz triangular
signal, 5 V pk-pk (29.4 mA), which resulted in approximately 38-43 GHz (or
0.3-0.4 nm) tuning. The modulation waveform had not been corrected, so the
scan of the laser is not linear, and the beat signal is therefore not constant
over the scan. At the distance of 40 cm, these parameters produced a beat
signal that was clearly visible at the time scale of the modulation period,
and this clearly illustrated the interference effect. The frequency of the beat
signal was also within the bandwidth of the detector for all the measured
distances, because the detector can detect frequencies up to approximately 2
MHz. From the peaks detected from the filtered signals, a comparison of the
time between two consecutive peaks gave an approximation to the instanta-
neous frequency, which illustrates the nonlinear scan of the laser. An FFT
is also presented for the 40 cm distance. The distance measurements were
done by following the method described in section 3.4. The filter used for
the distance of 40 cm is presented in figure 4.1. This filter had a passband
of 10-100 kHz. The filters used for the distances of 498, 930 and 1468 had

passbands of: 200-450 kHz, 550-750 kHz and 900-1,300 kHz, respectively. All FFT-spectrums presented here are the absolute value of the output from the FFT.

Section 4.2 presents the results in a more compact collection of plots, to more clearly illustrate the intermediate frequency and the Doppler shift.
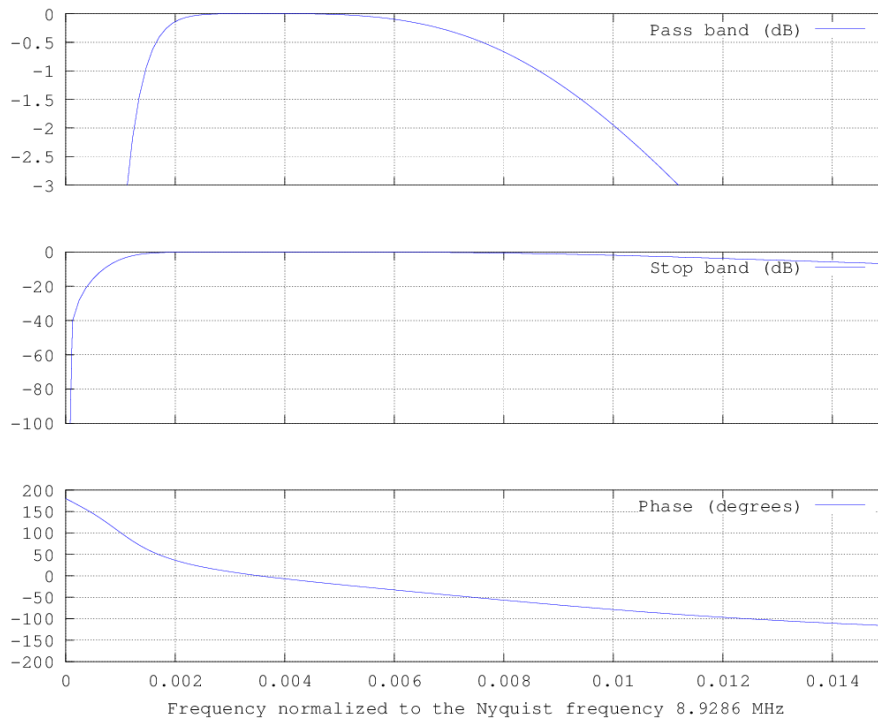
Figure 4.1: The filter used to remove low frequency noise from the modulation and high frequency noise outside the spectrum of the beat signal. Since the phase is affected by the filter, it is run both forwards and in reverse to achieve zero-phase digital filtering.

4.1   Signal at 40 cm distance

To test the system performance at a oscillating target, mirror M_1 was mounted on a 12" subwoofer(large speaker) from Biltema, driven by a custom ampli-

fier. This was controlled by a signal generator, which set the frequency to 0.5 Hz of triangular modulation and the amplitude to about 0.5 cm(1 cm pk-pk).

4.1.1 Static target

Using a stationary target figure 4.2 was produced. The time plot displays the signal that was used to calculate the FFT.
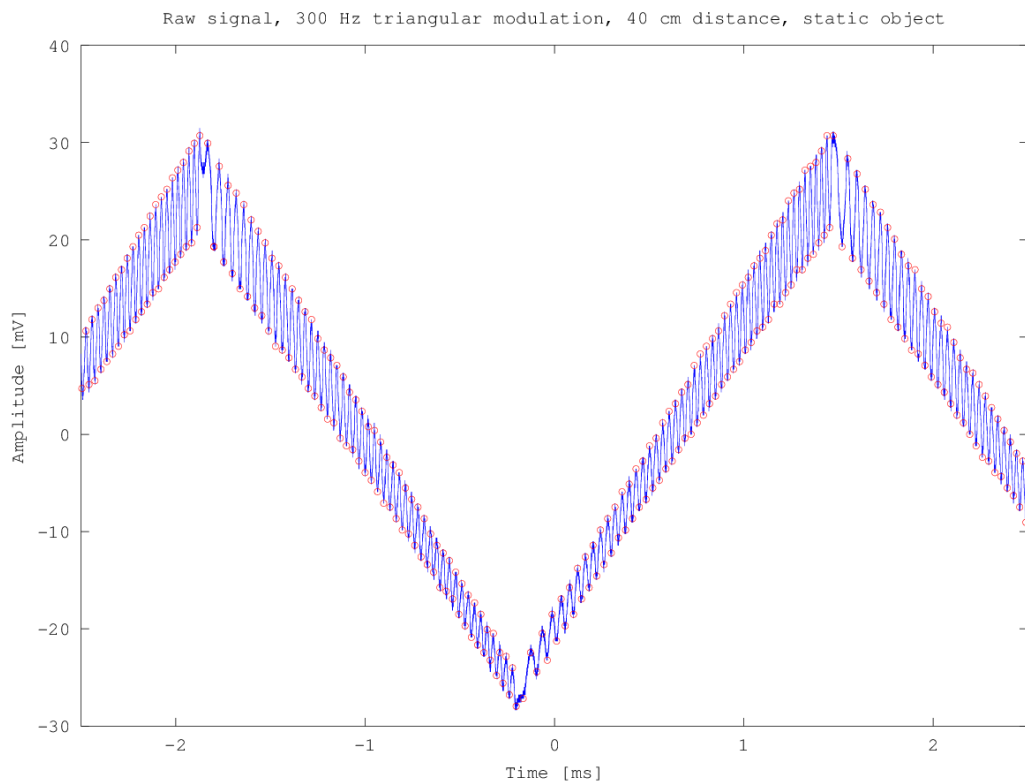
Figure 4.2: The raw signal detected at a distance of 40 cm, 300 Hz triangular modulation, static object. The modulation has not been compensated to create a linear scan of the wavelength of the laser. The peaks found from the filtered signal are marked in red.
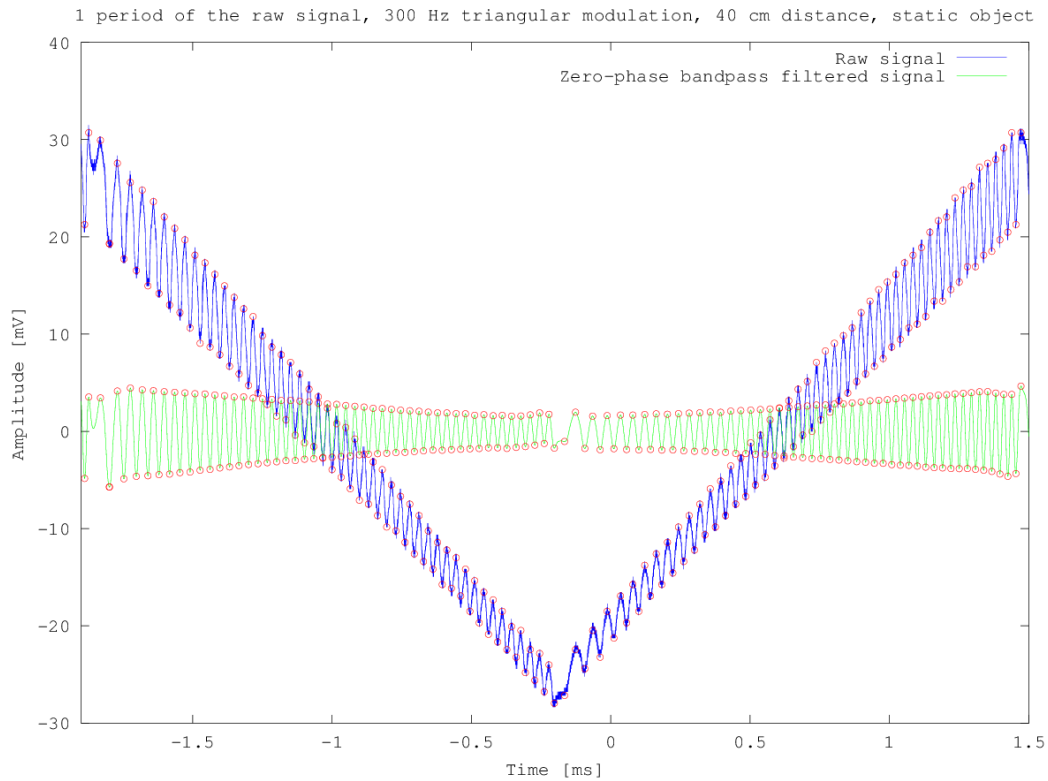
Figure 4.3: Plot showing one period of the raw signal(blue) in figure 4.2, along with the zero-phase filtered signal(green) and the peaks(red), which are found from the filtered signal, marked at both signals.

Figure 4.4 was constructed by subtracting the time of one peak from the following, for all the peaks shown in figure 4.3.
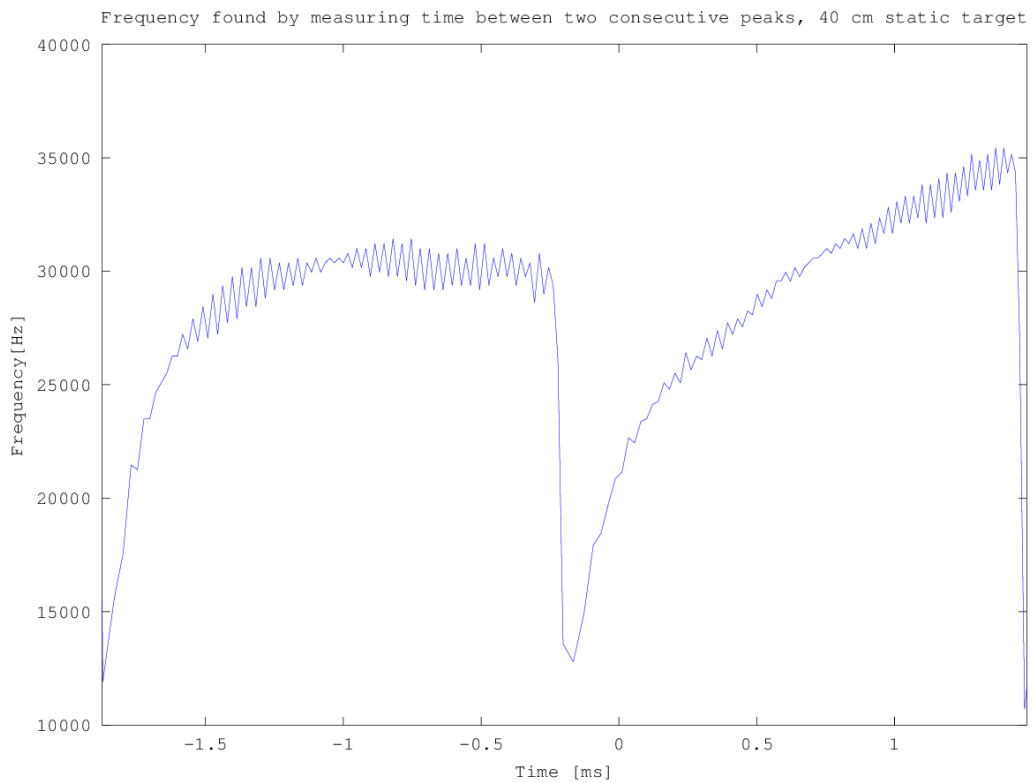
Figure 4.4: This plot shows the instantaneous frequency of the beat signal in figure 4.3. The frequency is found by determining the time between two consecutive peaks. Up to the time of approximately -0.2 ms represents the falling flank. For the data after approximately -0.2 ms, the data represents the rising flank.

Figure 4.5: Here the FFT of the raw(bus) and bandpass filtered signal(red) from 4.2 are plotted. The cut-off frequencies of the bandpass filter are 10 kHz and 100 kHz.

4.1.2 Target moving away from the system

With the target moving away from the system figure 4.6 was captured. The displacement was about 1 cm pk-pk, with a period of 2 second. This was done by applying a triangular 0.5 Hz signal to the subwoofer, and resulted in a velocity of approximately 0.01 m/s. Figure 4.7 show both the raw, filtered and zero-phase filtered signal in the same plot. First, the effect of a filter can be seen, and second the phase shift induced by applying a digital filter to a sample.

Figure 4.6: The signal from an object moving away from the system at a velocity of 0.01 m/s. The peaks marked in the plot were found by finding the peaks of the zero-phase bandpass filtered signal, shown in green.
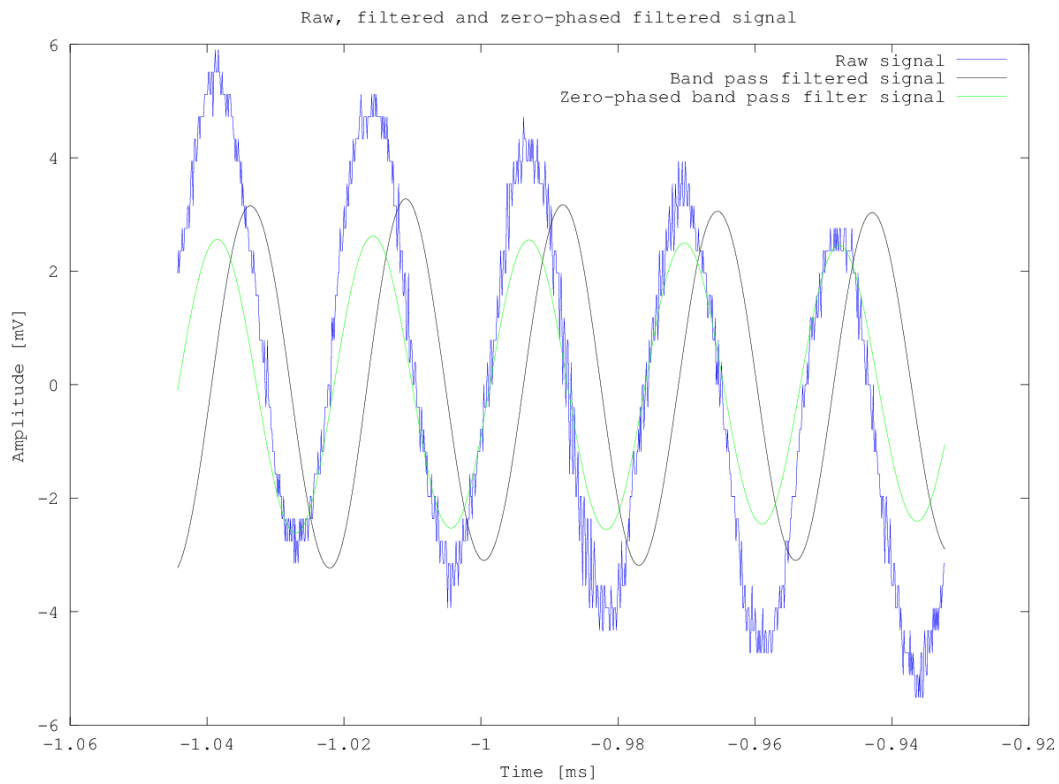
Figure 4.7: This is a zoomed in plot of the raw signal in figure 4.6, plotted along with the filtered signal, and the reverse filtered signal to achieve zero-phasing digital filtering.
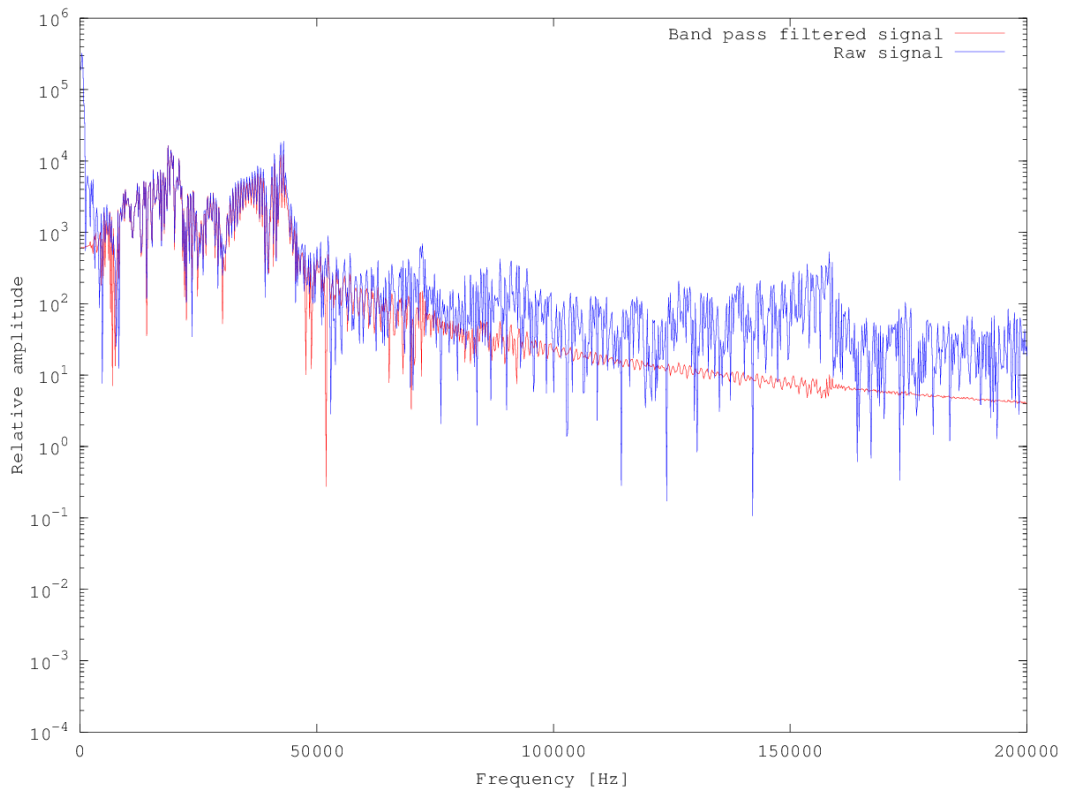
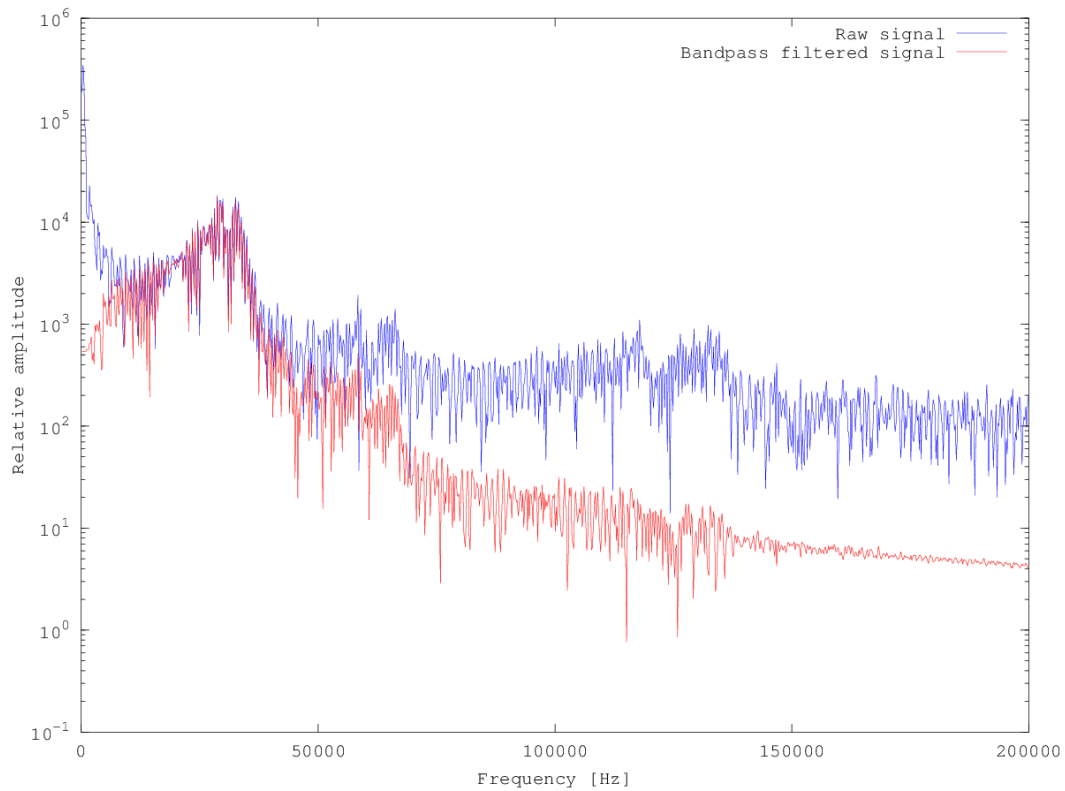Figure 4.8: Here the FFT of the raw(blue) and bandpass filtered signal(red) from 4.6 are plotted. The cut-off frequencies of the bandpass filter are 10 kHz and 100 kHz. Both the peak for the upshifted f_{if} in the falling flank, and the peak for the downshifted f_{if} in the rising flank are visible.

4.1.3   Target moving towards the system

With the target moving towards the system the data presented in figure 4.9 was sampled. The displacement was about 1 cm, with a period of 2 second. This was done by applying a triangular 0.5 Hz signal to the subwoofer, and resulted in a velocity of approximately 0.01 m/s. Figure 4.10 show both the raw, filtered and zero-phase filtered signal in the same plot. First, the effect of a filter can be seen, and second the phase shift induced by applying a digital filter to a sample.

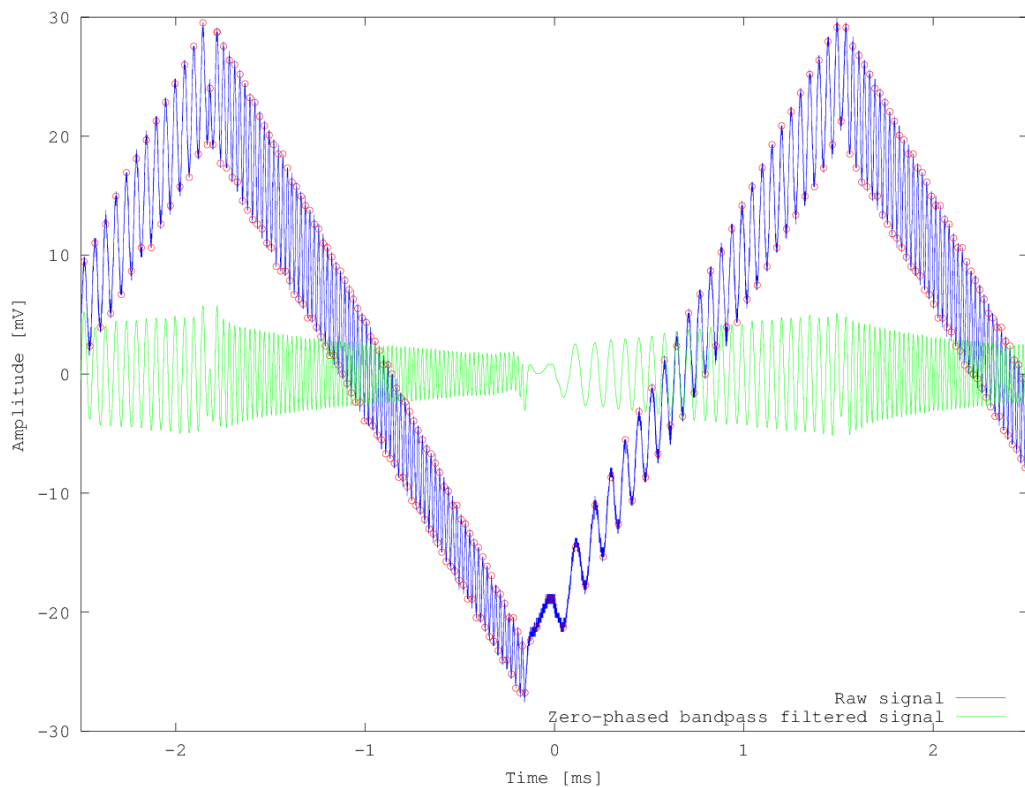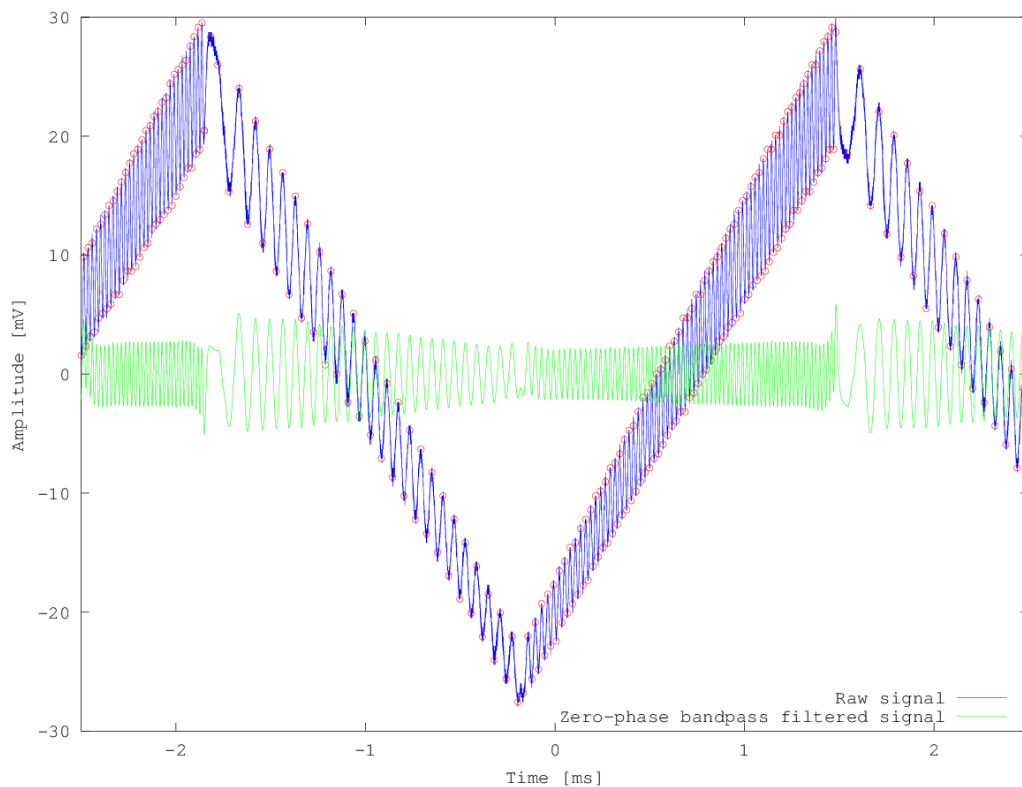Figure 4.9: The signal from an object moving towards the system at a velocity of 0.01 m/s. The peaks marked in the plot were found by finding the peaks of the zero-phase bandpass filtered signal, shown in green.
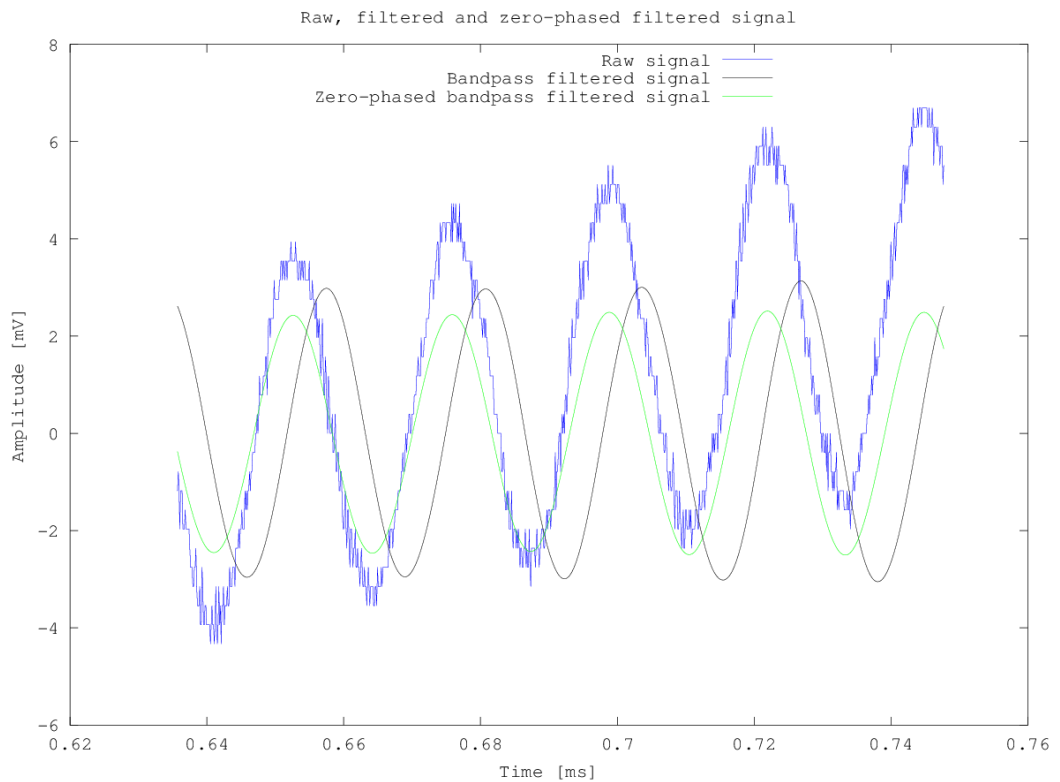
Figure 4.10: This is a zoomed in plot of the raw signal in figure 4.9, plotted along with the filtered signal, and the reverse filtered signal to achieve zero-phasing digital filtering.
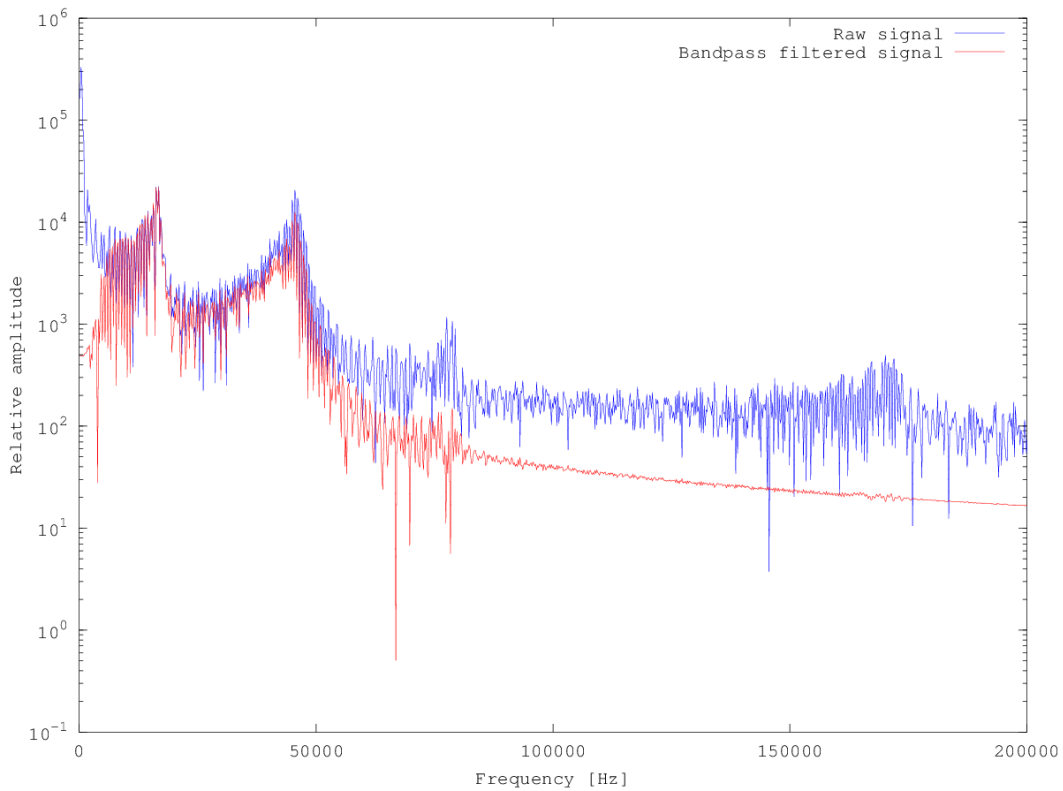
Figure 4.11: A plot of the FFT of the raw and bandpass filtered signal from 4.9. The cut-off frequencies of the bandpass filter is 10 kHz and 100 kHz. Both the peak for the downshifted f_{if} in the falling flank, and the peak for the upshifted f_{if} in the rising flank are visible.

4.2   Distance measurement

To produce the plots presented in this section, each falling and rising flanks were cut out from the filtered signals to avoid the fluctuations at each turning point. This is described in section 3.2. Note that the time plots for all distances above 40 cm are only a small part of the time signal that was used to calculate their FFT. This was done because the frequency of these beat signals are much higher than the measurement done at 40 cm. If the time plot was not magnified, the beat signal would look like noise in this time scale. The filter presented in figure 4.1 is only used for the distance of 40 cm. The cut-off frequencies were changed before applying the filter to the other measurements, because the beat frequency increases proportionally with the distance.

4.2.1   Target distance 40 cm

Measurement were done at a distance of 40 cm, for both a static and moving object. The time plot is a part of the filtered signal of the falling and rising flank in figure 4.2, 4.6 and 4.9. The time plot displayed for 40 cm is used to find the FFT, unlike the following distances where the beat frequency is much higher, and the time plot therefor had to be magnified.
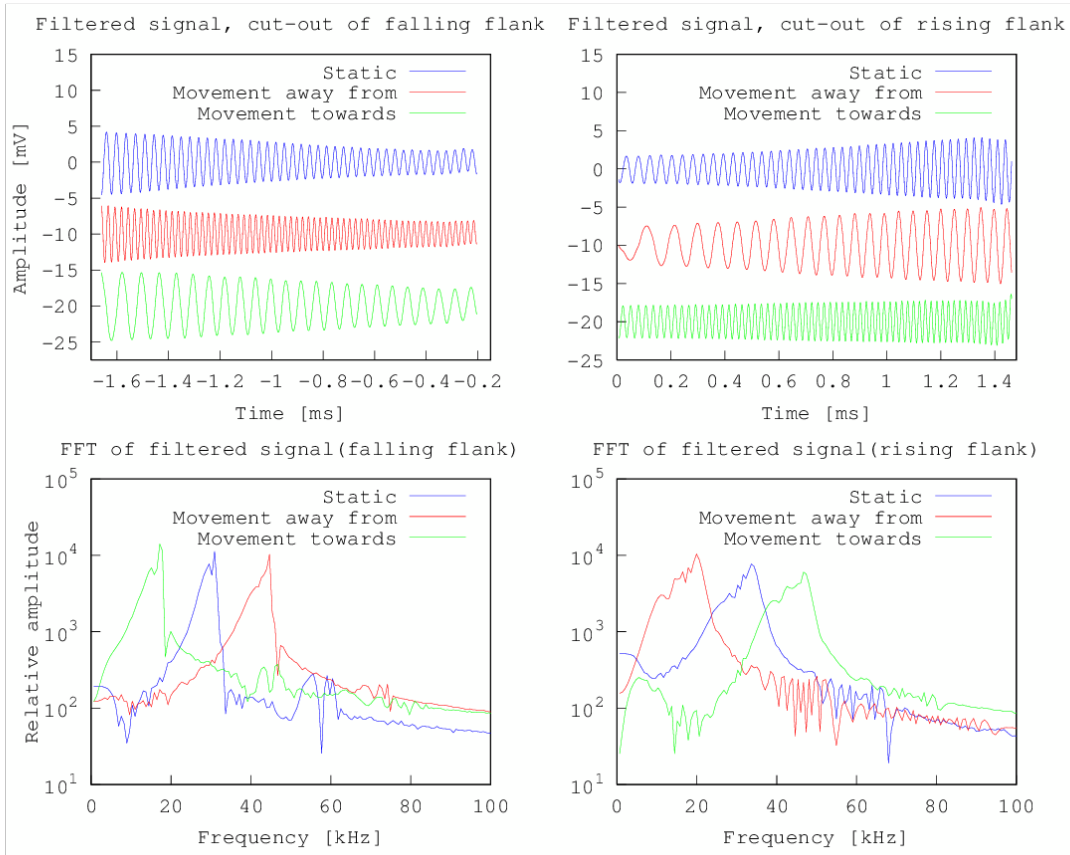
Figure 4.12: Results for measurements at 40 cm, both static and movement towards and away from. First the time measurements for falling and rising flank, and then FFT for these respectively. The falling and rising flanks were cut out from the filtered signals in figure 4.3, 4.6 and 4.9.

4.2.2 Target distance 498 cm

Measurement were done at a distance of 498 cm, for both a static and moving object.
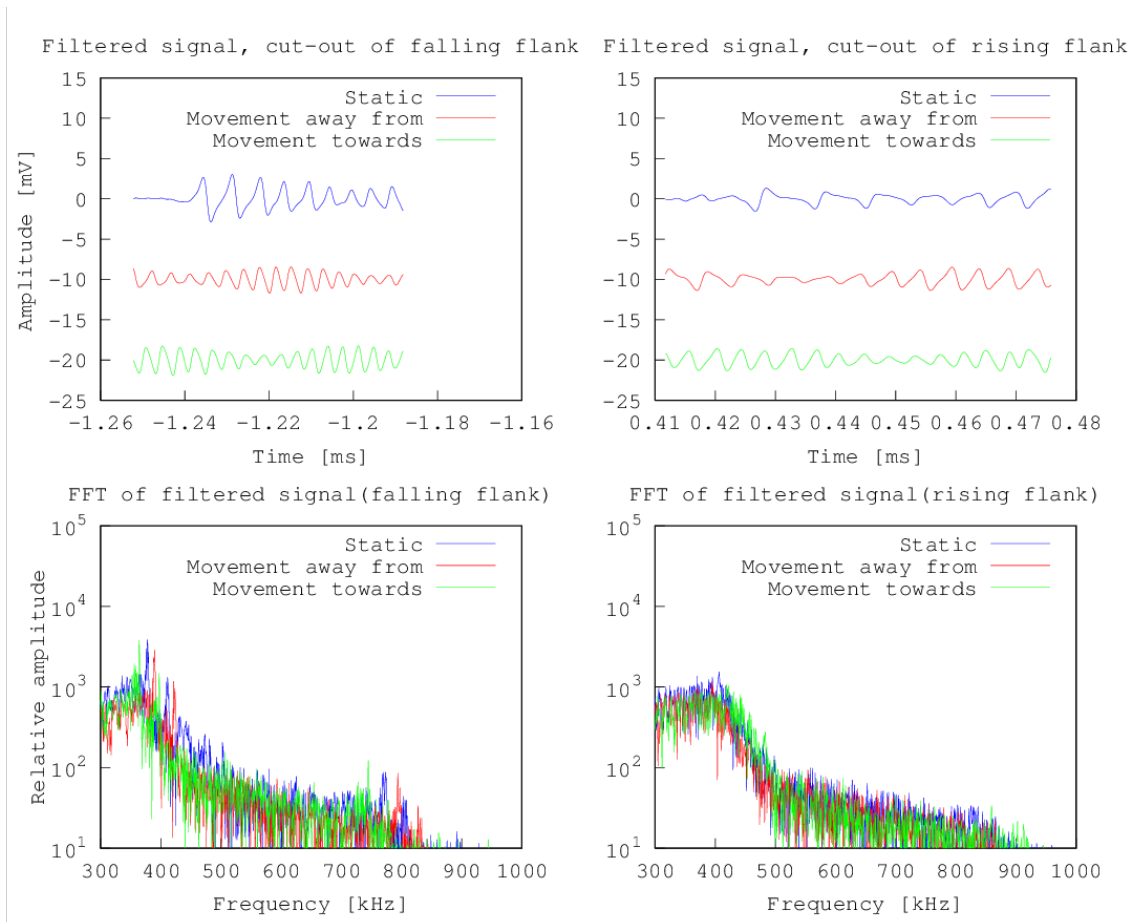
Figure 4.13: Results for measurements at 498 cm, both static and movement towards and away from. First the time measurements for falling and rising flanks are shown, and then FFT of these respectively. The falling and rising flanks were cut out from the filtered signals.

4.2.3   Target distance 930 cm

Measurement were done at a distance of 930 cm, but only for a object moving towards and away from the prototype, due to an error when saving the measurement data for the static measurement.
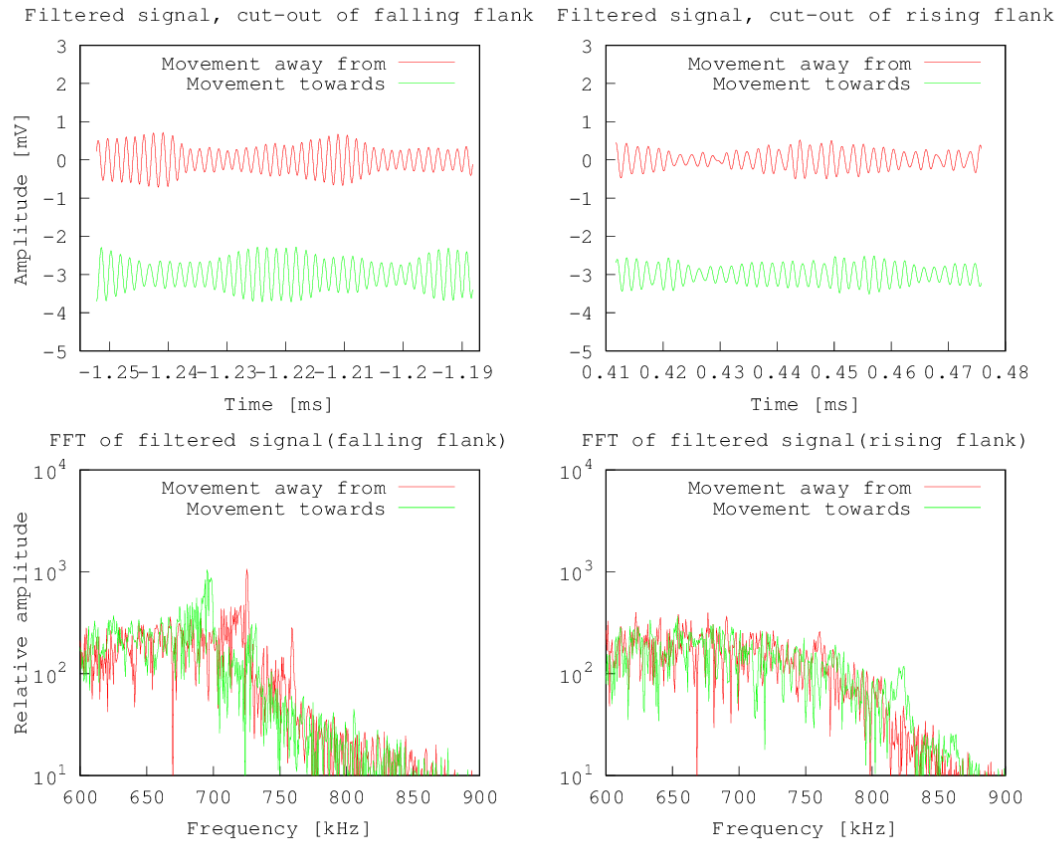
Figure 4.14: Results for measurements at 930 cm, only movement towards and away. No static data is shown due to an error when saving the measurement data. First the time measurements for falling and rising flank, and then FFT for these respectively. The falling and rising flanks were cut out from the filtered signals.

4.2.4 Target distance 1468 cm

Measurement were done at a distance of 1468 cm, for both a static and moving object.
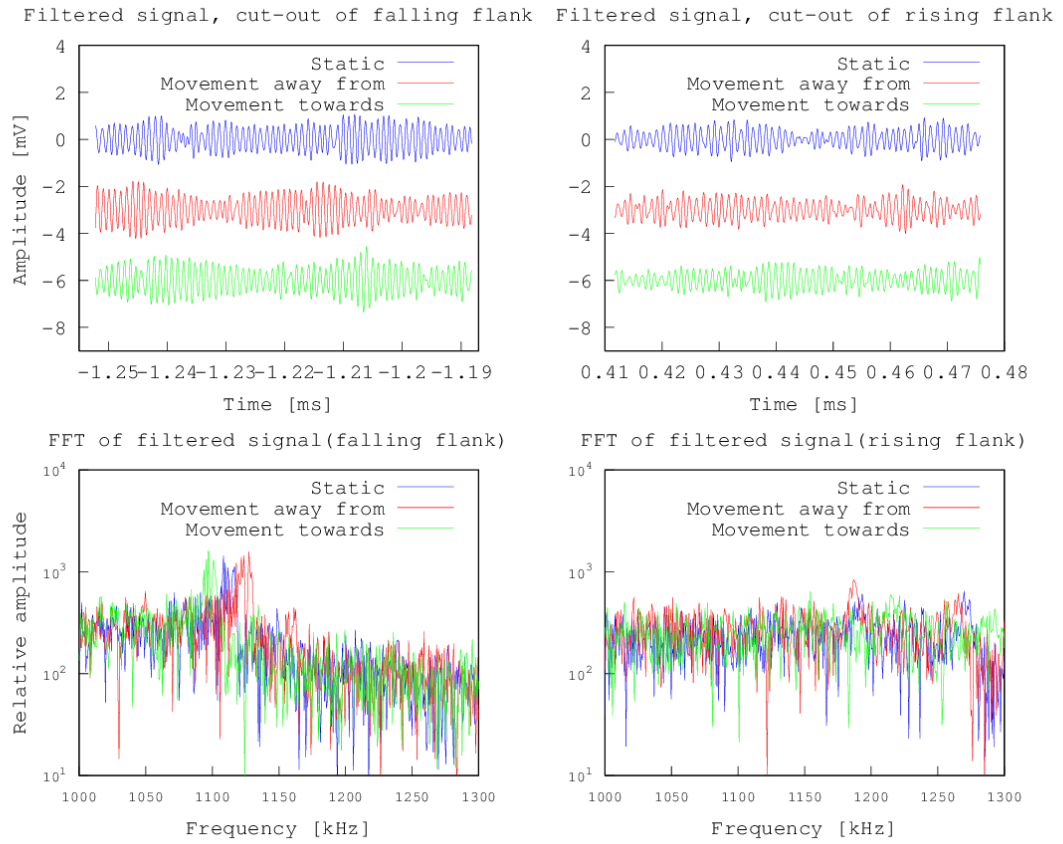
Figure 4.15: Results for measurements at 1468 cm, both static and movement towards and away. First the time measurements for falling and rising flank, and then FFT for these respectively. The falling and rising flanks were cut out from the filtered signals.

4.3 Tables of distance measurements and the intermediate frequency of the beat signal

An overview of the results plotted in the previous section are here presented in two tables. First, in table 4.1 the data for all of the falling flanks, second in table 4.2 the data for all of the rising flanks. In the tables *Distance* is the distance to the object from the setup, illustrated as R in figure 2.1. *Static*, *Away* and *Towards* refer to the movement of the object in relation to the

Distance [cm]	Away [kHz]	Static [kHz]	Towards [kHz]	Downshift [kHz]	Upshift [kHz]	Equiv. Δ f [GHz]
40	44.640	30.904	17.169	-13.736	13.735	38.630
498	389.652	377.536	364.143	-12.116	13.393	39.122
930	725.097	710.111*	695.125	-14.986*	14.986*	38.178*
1468	1,127.505	1,108.373	1,096.894	-19.132	11.479	40.423

Table 4.1: The data for the falling edge present in section 4.2 here. The measurements were made at 4 different distances, and with both a static and moving target. The velocity of the moving target was approximately 0.01 m/s. The position of the centre frequency was found by finding the highest amplitude of the FFT plotted for each measurement.

Distance [cm]	Away [kHz]	Static [kHz]	Towards [kHz]	Downshift [kHz]	Upshift [kHz]	Equiv. Δ f [GHz]
40	19.916	33.651	46.700	13.735	-13.049	42.064
498	394.117	406.871	418.988	12.754	-12.117	40.851
930	622.424	638.048*	653.672	15.624*	-15.624*	34.304*
1468	1,186.814	1,269.719	1,154.290	82.905	115.429	43.247

Table 4.2: The data for the falling edge present in section 4.2 here. The measurements were made at 4 different distances, and with both a static and moving target. The velocity of the moving target was approximately 0.01 m/s. The position of the centre frequency was found by finding the highest amplitude of the FFT plotted for each measurement.

system, and the value presented is the measured intermediate frequency, f_{if}. *Upshift* and *Downshift* refer to the Doppler shift, and is found by comparing the *Static* measurement to the moving one. *Equiv.* Δ f is the frequency scan of the laser light, which can be calculated from equation 2.9. Note that the measurements for the static object at the distance of 930 cm was lost due to an error. The value for static measurement at 930 cm(*) has therefore been estimated as the value in the middle of the frequency *Away* and *Towards*. The *Upshift* and *Downshift* has been calculated from this estimate, as has the *Equiv.* Δ f. The position of the centre frequency was found by finding the highest amplitude of the FFT plotted for each measurement.

Chapter 5

Discussion

To accurately determine the distance, the laser must be scanned linearly. Otherwise the intermediate frequency will not be constant over the modulation period.

5.1 Obtaining linear frequency ramping

As seen in figure 4.3 and figure 4.4 a linear triangular modulation current fed to the laser will not result in a linear wavelength tuning. This is due to the non uniform response of wavelength tuning to a modulated current supplied to the laser [13], and for the case of lower modulation frequencies($<$1 MHz) the dominant cause of this are the thermal fluctuations, as described by [18] and [20]. Without correcting for this nonlinearity the measurements will have to be corrected by post-processing the data. But there are several approaches to correct the waveform of the current to achieve linearity. One is to model the thermal components of the laser [18] [20], and another is to set up the system to a specific distance, connect the detector signal to a lock-in-amplifier and feed this signal back to the driving current to the laser [13]. This creates a phase-locked loop which will correct the frequency of the beat signal when it deviates from the reference. These techniques were not tested

in this thesis but should be considered for future work. In the plots presented in section 4.2 the falling flank gives a more distinct peak for the intermediate frequency for all the distances. This is due to the falling flank being closer to a linear scan than the rising flank, which can be seen by the more constant f_{if} in figure 4.4 for the falling flank than the rising flank.

5.2 Measurements at 40 cm

5.2.1 The velocity of the moving object

The velocity of the moving object is determined by both the frequency and the amplitude of the oscillation. The triangular oscillation was set to a frequency of 0.5 Hz, and the amplitude was measured to be about 0.5 cm(peak to peak 1 cm). For an object moving away from the system this should result in the following Doppler shift:

$$
\begin{aligned}
f_D &\approx -\frac{2v}{\lambda} \\
&= -\frac{2 \cdot 0.01}{1595 \cdot 10^{-9}} \\
&= -12,539 \ [\text{Hz}].
\end{aligned}
\tag{5.1}
$$

From the upshifts and downshifts in table 4.1 and 4.2 the actual velocity can be calculated. Since the measurements were less accurate for the longer distances, which can be seen by the wider tops in the FFT in figure 4.14 and 4.15, these were left out. The average of the upshift and downshift is 13.079 kHz(based on the values: 13.736, 12.116, 13.735, 13.393, 13.735, 13.049, 12.754 and 12.117 kHz). This results in the velocity:

$$
\begin{aligned}
v &\approx \pm\, \frac{f_D \cdot \lambda}{2} \\
&= \pm\, \frac{13,079 \cdot 159510^{-9}}{2} \\
&= \pm\, 0.010431... \\
&\approx \pm\, 0.01\ [\mathrm{m/s}].
\end{aligned}
\tag{5.2}
$$

The detected velocity, and therefor the amplitude of the oscillation, was therefor very close to what was expected. The only other inaccurate variable in this equation is the wavelength, which was not measured with the spectrum analyzer as this instrument is situated in Trondheim, and the project was at this point moved to Oslo/Lørenskog. The approximate λ was set to 1595 nm, which is the middle of the interval given in the data sheet. If the real value in fact were different than this, the deviation would not be large, as the interval is from 1565-1625 nm, which is only a 3.8 % deviation.

So this experiment proves that the Doppler shift can be detected with this setup. It is clear from the measurements that the effect was detected and it is shown that this can be used in the optical FMCW setup to measure small oscillations.

5.2.2   Operating sensitivity to oscillations

The measurements of the target done at 40 cm show several important phenomena. As already described, the nonlinear scan of the wavelength of the laser can be seen in figure 4.2. The Doppler shift induced from the mirror mounted on the moving subwoofer membrane can be seen in figure 4.6 and 4.9. A velocity of about 0.01 m/s induced the shifts seen in the two figures. The shift was approximately 13 kHz, which is detectable with this setup. If a bridge were to oscillate as a sine waveform at 4 Hz, with a distance of 0.1 mm between the maximas, the velocity would be

$\frac{d}{dt}[0.510^{-4}\sin(2\pi 4t)] = 4\pi 10^{-4}\cos(2\pi 4t)dt = 0.0012566$ [m/s]. The corresponding Doppler shift would be:

$$
\begin{aligned}
f_D &= \pm\frac{2\cdot 0.0012566}{1595\cdot 10^{-9}} \\
&= \pm 1575.7 \text{ [Hz]}.
\end{aligned}
\tag{5.3}
$$

Therefore the specification of detecting small displacements down to 0.1 mm can be reached with a system based on the optical FMCW combined with detecting the Doppler shift. The resolution will be worse if the frequency the object oscillates with is reduced. However, if the frequency shift in equation 5.3 is detectable, then a 1 mm displacement would be detectable when an object oscillates with only 0.4 Hz. From the eigenfrequency analysis of a concrete bridge in appendix A, it is clear that expecting a frequency of some Hz for the oscillation of some bridges is not unrealistic. This eigenfrequency is related to the stiffness of the construction, and the material and dimension, but can be in the ball park area of 1-10 Hz. It is still possible that the absolute distance resolution could reach the goal of 0.1 mm resolution at distances up to 25-30 meters. But the prototype built in this project will fulfil the resolution requirement or be close to it, and might have an absolute resolution down to cm-range. This will make it possible to log and detect slow changes in position, like a bridge expanding when struck by sunlight, and contracting when the temperature goes down during the night. The system built in this project can therefore meet both requirements of resolution set in the problem description. Note that the Doppler shift will be higher for a shorter wavelength, so changing the laser to a laser with $\lambda = 760$ nm will approximately double the frequency shift. When operating with a modulation frequency of 300 Hz, collecting 300 samples for the falling flank and 300 samples for the rising flank every second, the system will be more than fast enough to monitor oscillations of up to 10 Hz. The limit for detecting oscillations is governed by the Nyquist-Shannon sampling theorem, which states that the sampling rate has to be larger than twice the highest frequency that

is sought to detect. In practice one might need more than just above 2 times the highest frequency, but in this case the factor is 30 which will make it easy to log and follow changes in the position of the oscillation.

5.3 Operating distance

From the measurements of the target at 40 cm, the Doppler shift proved to be about $\pm$ 1/2 of the intermediate frequency. If the distance were to be set to about 17 cm, the carrier frequency(f_{if} of static measurement) would be around 13 kHz, which is close to the Doppler shift experienced in the tests done in chapter 4. The Doppler shift would in that case give close to 0 Hz for one of the shifts, and close to 26 kHz for the other, depending on the measurement being done on the falling or rising flank. Measuring a signal close to 0 Hz would be difficult because of all the frequency components of the modulation. These exist because the intensity of the laser is tuned along with the frequency, but can be filtered out if the frequency of the beat signal is much higher than the strongest frequency components of the modulation. The Fourier series of both the sawtooth waveform and the triangular waveform were included in section 2.2 because they show that the frequency components of the triangular waveform decrease as $1/n^2$, while the sawtooth only decreases as $1/n$. In addition, the slope of the triangular waveform is twice as steep as the sawtooth waveform for the same pk-pk and period. The triangular modulation will therefore only have frequency components in the lower spectrum, and can easier be filtered out from the beat signal. However, decreasing the modulation period or increasing the wavelength scan of the laser will increase the intermediate frequency, making it possible to measure smaller distances without the Doppler shift moving lowering the beat signal too much. But if the bandwidth of the detector is not high enough, this will increase the resolution of the optical-FMCW for displacements at shorter distances but limit the operating distance. So the minimum distance is not a practical obstacle for the task of monitoring oscillations and displacements in structures. The maximum distance is on

the other hand important. A system that can only work at distances of a few meters is not very practical for most bridge spans. The maximum distance measured with this setup was 14.68 meters. This does not fulfil the operational distance requirements set in the problem description, which was 25-30 meters. A signal was detectable at about 20 m distance when lowering the modulation frequency to 100 Hz triangular modulation, and lowering the voltage of the modulation to 1 V pk-pk. This indicated that the coherence length is not the limiting factor for the final setup. Initially, using laser 1 with a coherence length of only 15 meters, the beat signal was lost just before 3 meters. Changing to Laser 2 with a coherence length of 150 meters, distances up to 7 meters were possible to measure. The results were improved by changing the collimating lens to a doublet, making sure the beam was well collimated. It is also important that the intensity is uniform over the entire cross section of the beam. It was when using this setup that measurements of oscillations of 1 cm movement (pk-pk) at 0.5 Hz in the Z direction was done at distances up to 14.68 m. The main suspect for not reaching a longer distance with this setup is still the collimation of the beam. The decreasing amplitude of the signal in the figures in section 4.2 is an indication of this. In addition to lowering the intensity of the object beam before it is reunited with the reference beam, the divergence can cause back reflection into the laser which will result in more noise. A steeper scan of the laser might be more sensitive to added noise, so this could be a reason why the standard parameters used in the other measurements did not yield a noticeable signal, but lowering the modulation from 300 Hz to 100 Hz, and the scan of the laser from 5 V pk-pk to 1 V pk-pk, resulted in a very weak signal at approximately 20 m.

The bandwidth of Detector 2 is not thought to be the limiting factor, as it is sensitive to approximately 2 MHz with the custom amplifier supplied from NEO. It could on the other hand reduce the SNR when the signal is close to 2 MHz, which together with the other losses from the divergence of the beam and a lower degree of coherence, could be a part of the problem. For a final setup the bandwidth should be increased in the detection unit. There

are several components available on the market, like Detector 1, that have a bandwidth up to GHz.

Another challenge that was faced was that the laser beam appeared to oscillate up and down when the distance was increased above 2-3 m. The measurements on the oscilloscope even fluctuated to some degree. But it was difficult to see the laser beam because of it being in the IR-spectrum, and the collimated beam having a low intensity distributed over some square cm. After some time the source of this fluctuation was found to be a piezo element mounted on the laser to avoid some problems with Fabry-Perot etalon reflections. The effect of using the piezo was decided to be unfortunate for this prototype, and disconnected from the power supply.

5.3.1 Absolute distance

Even though the absolute distance was not measured for small changes in R, except for oscillating targets, it can still be approximated. The distance of 40 cm resulted in a beat frequency of 30.904 kHz for the falling flank. This equates to 772.5 Hz per cm. If the setup is presumed to be sensitive to changes of 1.5757 kHz, which is the Doppler shift in equation 5.3, then a change in absolute distance of about 2 cm is resolvable. This should be tested in future work, when both the setup and detection method has been optimized.

5.4 Sources of error

To produce the plots in chapter 4.2 and tables in section 4.3, a part of the flank was chosen manually to avoid the shift occurring right after the peaks in the triangular waveform. Note that this shift is for the most part a result of the thermal fluctuations of the laser, as the undefined region, as described in 2.3 for the sawtooth waveform, will be only 200 ns for the distance of 30 m. The manual selection of the samples may have resulted in some differences

between what part of the flank that was chosen for the three different signals plotted together. Because of the nonlinearity of the scan, comparing different parts of the flank to each other will cause an error. This can be seen in figure 4.4, where the intermediate frequency is plotted versus time. If the intermediate frequency at one point in time is compared to the intermediate frequency at another point in time, the result will not be accurate. To avoid this, a trigger from the signal generator can be used find a universal trigger point.

The absolute distance of the measurements taken were also not accurate enough, so in reality the real distance is probably incorrect with up to $\pm$ 2.5-5 cm, increasing with an increasing distance. It could be argued that for the beat signal to accurately determine the position, the scan of the laser first need to be linearised. But it would anyway be valuable to have known the real distance more accurately. The oscillations and their frequency were detected anyway, and the inaccuracy of the absolute distance was constant for all the measurements done at a specific distance, meaning that they were not time dependent.

The signal might not have been optimised because the wavelength of Laser 2 was in the IR-spectrum and only some mW in intensity. This made it difficult to align the setup very accurately, so the signal might be weaker than what was possible to achieve. Both the collimation, overlapping of the reference and reflectance beam and centring the beams on the optical axis might be slightly incorrect. In a final setup an optical isolator should be considered to avoid back reflection and noise in the laser. Because this reduces back-reflection into the laser, it can positively affect the coherence length which will improve the SNR.

The components used are of course better suited for some wavelengths than other wavelengths. For Laser 1 BS 1 had approximately a reflection of 59 % and a transmission of 36 %. The retroreflectors had a reflectance of about 68-72 % for Laser 1, which was probably even lower for the wavelength of Laser 2. Using retroreflectors and a 50:50 BS that are almost lossless for

the wavelength of the laser should improve the SNR. If a sapphire or glass window is still chosen, one with an anti-reflective coating on one side for the relevant wavelength should be picked, or with a wedged shape to separate the front side and back side reflections. The lenses should also be swapped with ones that have anti-reflective coatings and a low loss for the relevant wavelength.

The setup also needs to be field tested, which could reveal challenges with moisture, dust, sunlight/bright light, placing the setup at a fixed position to avoid detecting its own vibration, and probably several other more or less important problems.

Chapter 6

Conclusion

To be able to both measure an absolute distance and small displacements the technique of optical FMCW range finding was examined and a prototype was built. In combination with measuring the distance, the Doppler shift is utilized to measure small displacements. This is like a LDV, but with the intermediate frequency from the FMCW used instead of a Bragg cell to shift one of the arms of the interferometer.

The setup was able to measure absolute distances up to approximately 15 m. This is about half the target of 25-30 m, which should be reachable. The reasons why this distance was not achieved are thought to be mainly because of non optimal collimation and alignment. The components can also be changed out with components that are optimal for the wavelength of the laser to achieve a higher SNR. This was not done in this project due to the change of the laser at a late stage and a limited access to equipment. The detector bandwidth of approximately 2 MHz is not the limiting factor, but could be contributing to a lower SNR when the beat frequency approaches 2 MHz. Measuring absolute distances of 25-30 m with Laser 2 is feasible by optimising the setup(Laser 1 was on the other hand not suitable, because the coherence length of 15 m is too short). Tests done with Laser 2 at 20 m with

lower current modulation(and therefore Δf), and lower modulation frequency produced a signal with a small but noticeable SNR. This can indicate that the coherence length is not the limiting factor, but instead back reflection into the laser, possibly caused by the divergence of the beam, is limiting the lasers operational distance.

The setup detected triangular oscillations of a subwoofer at 0.5 Hz, with a peak to peak movement of 0.010430 m at distances between 0.4 m and 14.68 m. The results from these measurements indicate that a small vibration of i.e. a bridge should produce a detectable frequency shift. Specifically the sinusoidal oscillation of 4 Hz will make the system sensitive enough to reach the target of 0.1 mm peak to peak movement, which results in a Doppler shift of about 1.58 kHz. When presuming that a change of 1.58 kHz in the beat frequency is detectable, a change in the absolute distance of 2 cm will be detectable with this setup.

The system proposed still needs a lot of development to be practical for monitoring structures at greater distances and with a better resolution. Signal processing also has to be developed and integrated to make it capable of operating in real-time. The principle of building the system on an optical FMCW technique, along with utilizing the Doppler shift, is tested and proven be sufficient for health monitoring of structures. Both long term variations of position and short term oscillations of small displacement can be measured with the Doppler shift FMCW setup.

Chapter 7

Future Work

There are several possible improvements to the setup so that the requirements of distance and resolution are met.

- Changing the detector and/or the bandwidth of the amplifier to enable a higher bandwidth, possibly up to GHz bandwidth.

- Better collimation of laser beam/changing to a higher quality lens.

- Changing the laser to one with a longer coherence length.

- Using an optical isolator instead of cube corners for avoiding back-reflection into the laser.

- For improved Doppler resolution, change to a shorter wavelength laser.

- Building an optimised system for signal processing to sample several 10's or 100's samples every second to detect oscillations.

- Compensate the modulation of the laser(scanning of wavelength) to scan the laser linearly.

- Change components that are unsuited for the wavelength of the laser.

Appendix A

Eigenfrequency analysis of a bridge

The following analysis is an eigenfrequency analysis of a bridge. The bridge is 68.99 m long, supported by two columns, one rigid and one free connection. The first eigenfrequency mode of this bridge is at 3.503 Hz. This bridge is designed after the new guidelines in Statens Vegvesen N400. The analysis was performed by M.Sc. Civil and Environmental Engineer Sindre Martin Hermstad, at COWI AS.

Eurocode

68.99

20.26　　　26.92　　　21.81

11.00

Eurocode

68.99
26.92
21.81
11.00
20.26
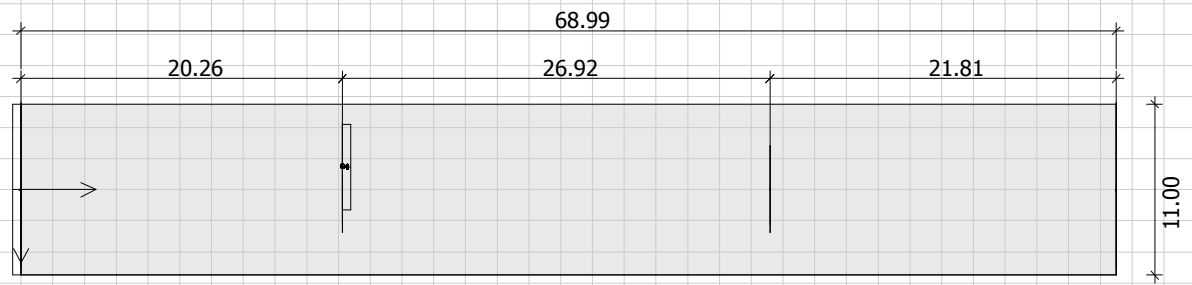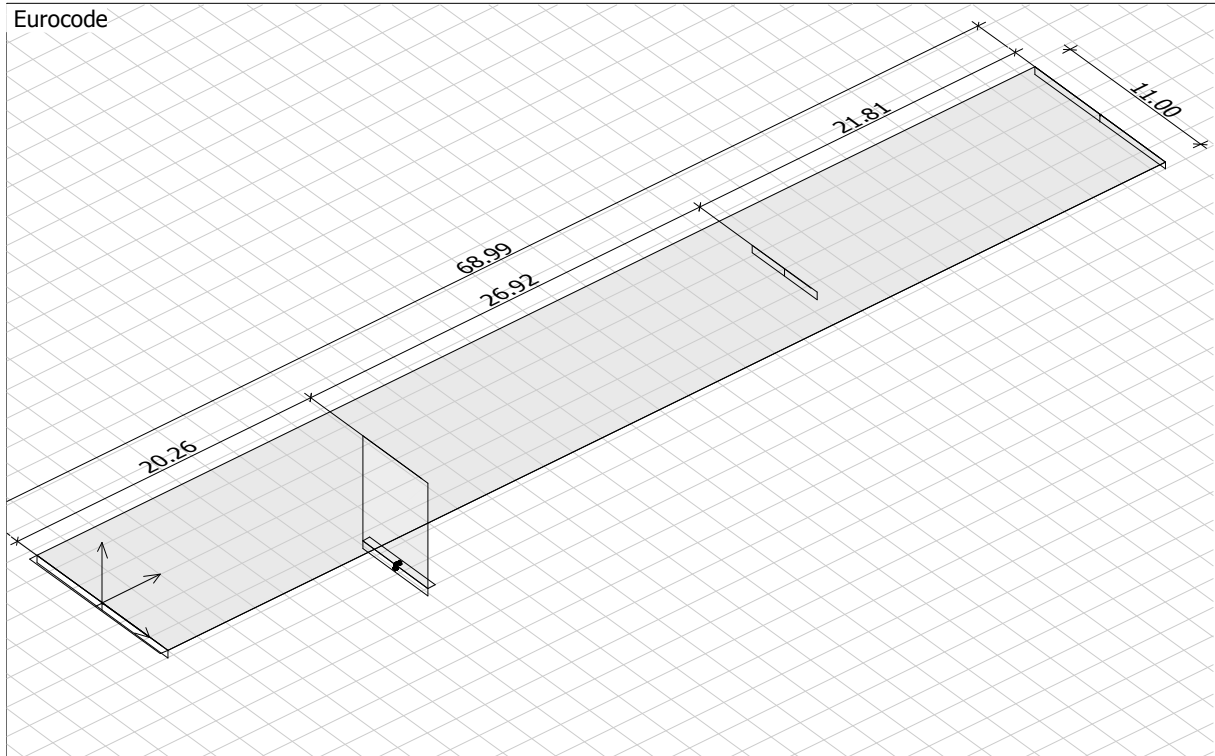
Project:	Customer:
Typical reinforced concrete plate bridge	NTNU
Description: Eigenfrequency analysis	FEM-Design 13 © StruSoft
Designed: SMHE	Date: 06.08.2014　Page: 1 / 6

This document describes a two lane, 70 meter long, three span, concrete plate bridge without prestressed concrete. This example is loosely based on an ongoing COWI project. The bridge is typical regarding design and length, and this analysis will therefore be suitable as an example that can represent other concrete bridges with similar length and width, where frequency values are in focus.

Simillar bridges will have similar or higher eigenfrequencies than the results presented here.

The obtained results are only suitable as an approximate evaluation of the eigenfrequencies and modal responses for the given bridge, and may not be used for actual design purposes.

2 Model

Concrete materials

No.	Name	Fck	Fctm	Fctk	Ecm	Yield strain	Ultimate strain
[-]	[-]	[N/mm2]	[N/mm2]	[N/mm2]	[N/mm2]	[-]	[-]
1	C45/55	45.000	3.800	2.700	36000.000	0.00175	0.00350

Gamma c	Gamma c, acc	Gamma cE	Gamma s	Gamma s, acc	Alfa cc	Alfa ct	Density
[-]	[-]	[-]	[-]	[-]	[-]	[-]	[t/m3]
1.50	1.20	1.20	1.15	1.00	1.00	1.00	2.548

Therm. coeff.	Poisson's ratio	Environ. class	Creep coefficient	Shrinkage
[1/°C]	[-]	[-]	[-]	[-]
0.000010	0.200	X0	0.000	0.000

Dyna r.
[-]
1.000

Plates

ID	Material	t1	t2	t3	E2/E1	Alpha	Ecc.	Ecc. calc.	Ecc. crack.
[-]	[-]	[m]	[m]	[m]	[-]	[rad]	[m]	[-]	[-]
P.1.1	C45/55	1.100	1.100	1.100	1.000	0.000	0.000	No	No

Walls

ID	Material	t1	t2	t3	E2/E1	Alpha	Ecc.	Ecc. calc.	Ecc. crack.
[-]	[-]	[m]	[m]	[m]	[-]	[rad]	[m]	[-]	[-]
W.1.1	C45/55	0.800	0.800	0.800	1.000	0.000	0.000	No	No

Line support groups

ID	Kx' comp.	Kx' tens.	Ky' comp.	Ky' tens.	Kz' comp.	Kz' tens.	Cx' comp.	Cx' tens.
[-]	[kN/m/m]	[kN/m/m]	[kN/m/m]	[kN/m/m]	[kN/m/m]	[kN/m/m]	[kNm/rad/m]	[kNm/rad/m]
S.1	1.00E+007	1.00E+007	1.00E+007	1.00E+007	1.00E+007	1.00E+007	0.00E+000	0.00E+000
S.3	1.00E+010	1.00E+010	1.00E+010	1.00E+010	1.00E+010	1.00E+010	1.00E+007	1.00E+007
S.4	1.00E+007	1.00E+007	0.00E+000	0.00E+000	1.00E+007	1.00E+007	0.00E+000	0.00E+000

Cy' comp.	Cy' tens.	Cz' comp.	Cz' tens.	Type	Disconn.
[kNm/rad/m]	[kNm/rad/m]	[kNm/rad/m]	[kNm/rad/m]		
0.00E+000	0.00E+000	0.00E+000	0.00E+000	-	No
1.00E+007	1.00E+007	1.00E+007	1.00E+007	-	No
0.00E+000	0.00E+000	0.00E+000	0.00E+000	-	No

3 Finite element mesh

Finite element Mesh

Eurocode

11.00

21.81

68.99

26.92

20.26

1 m

4 Mass model

20.26

68.99

26.92

21.81

11.00
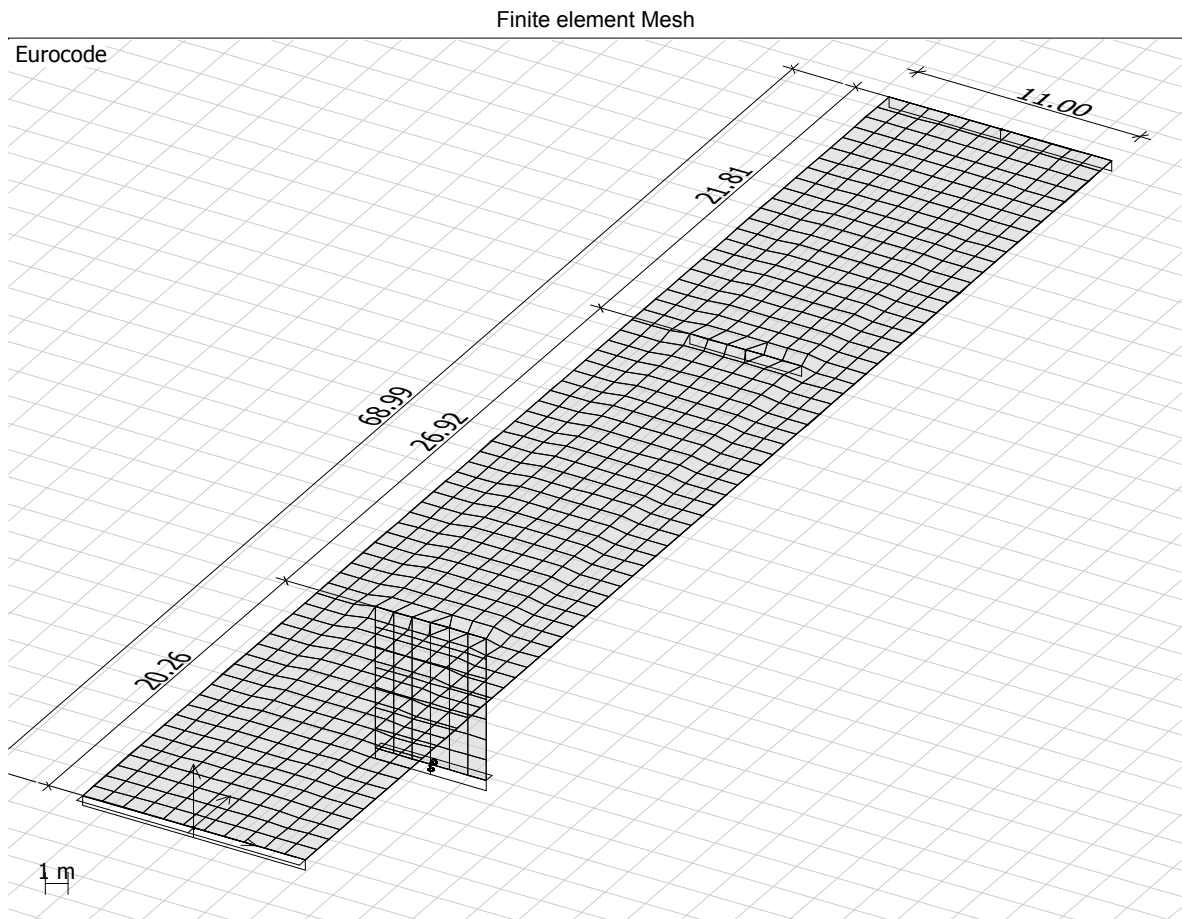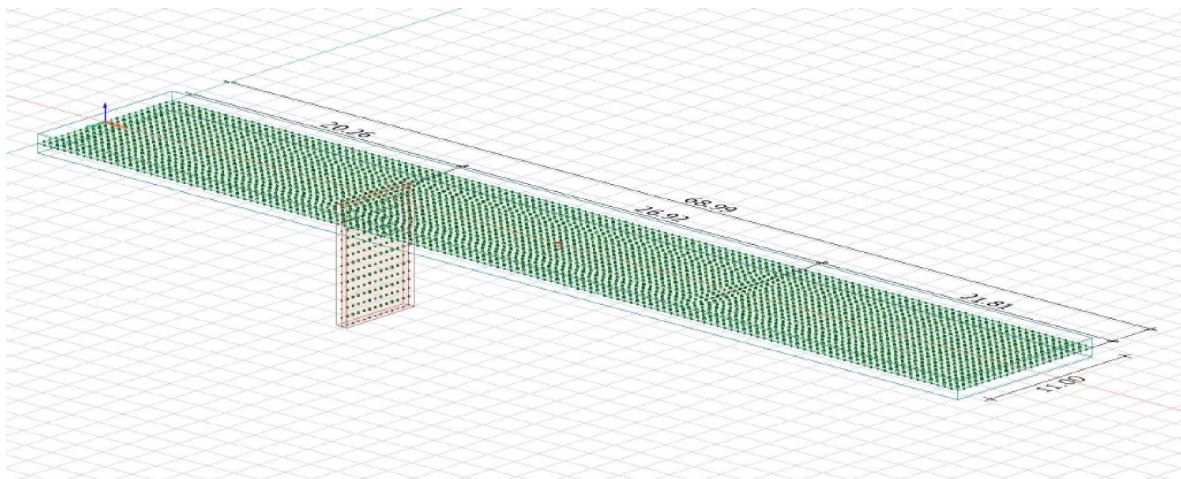
5 Results

Eigenfrequencies

Shape	Frequency	Period
[-]	[Hz]	[s]
1	3.503	0.286
2	5.278	0.189
3	6.382	0.157
4	6.664	0.150

Mode shape 1, view 1
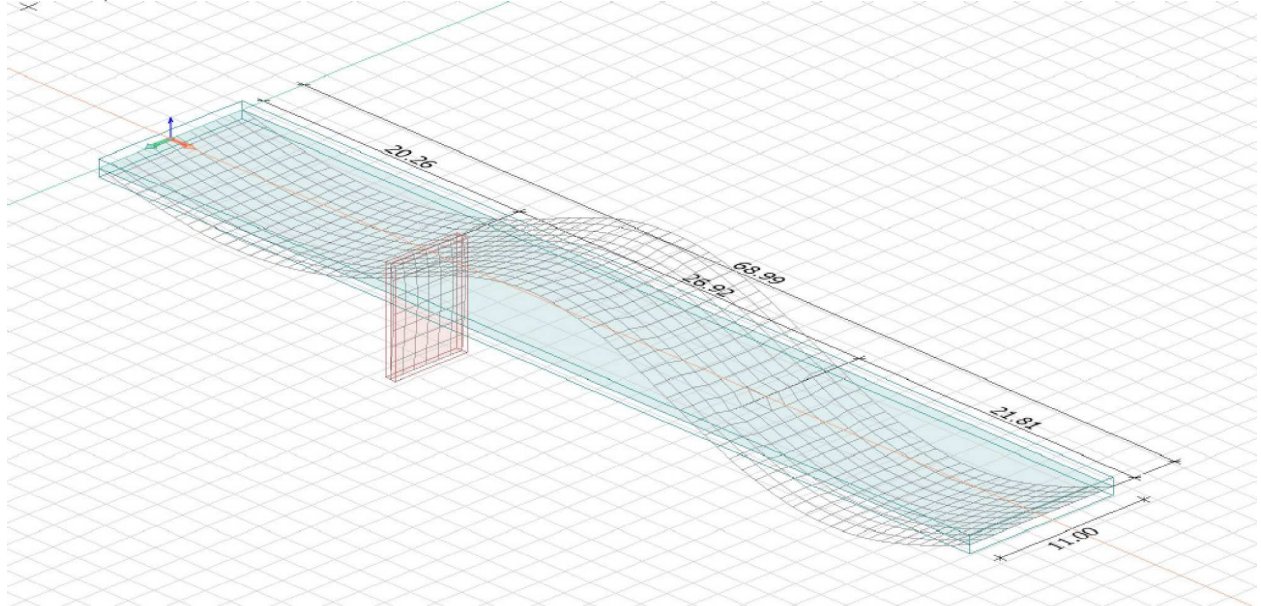
Mode shape 1, view 2

Mode shape 2

20.76

68.99

26.92

21.81

11.00
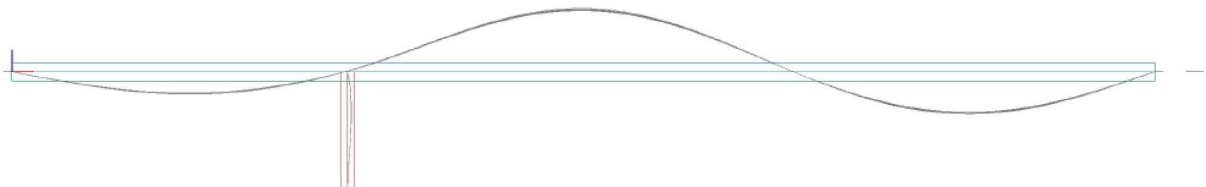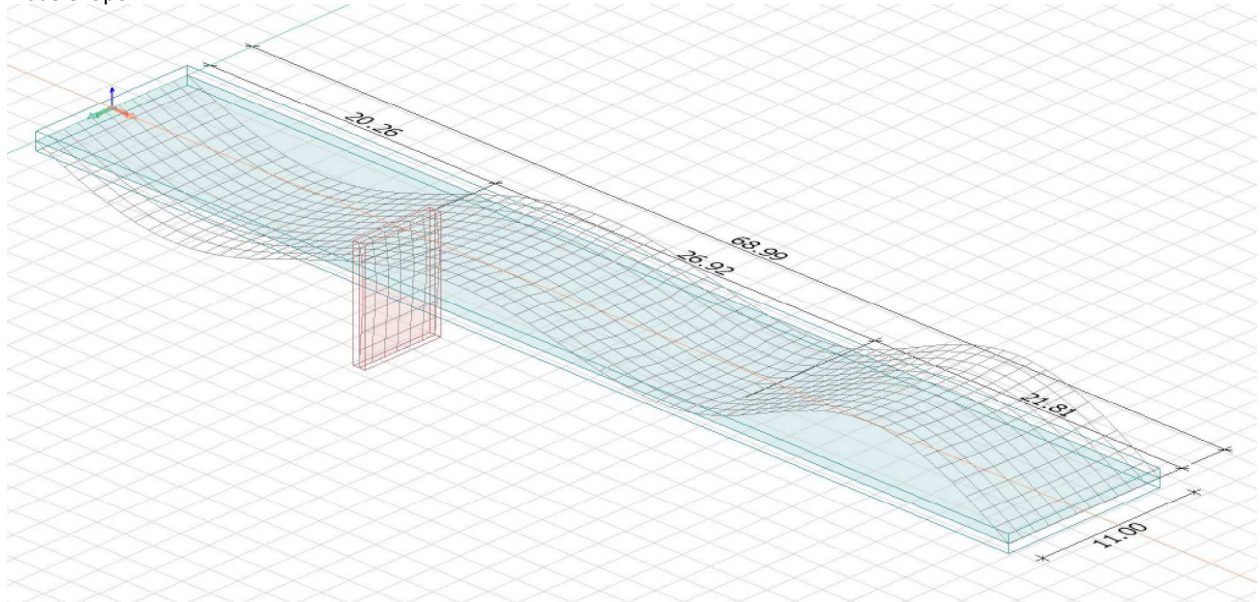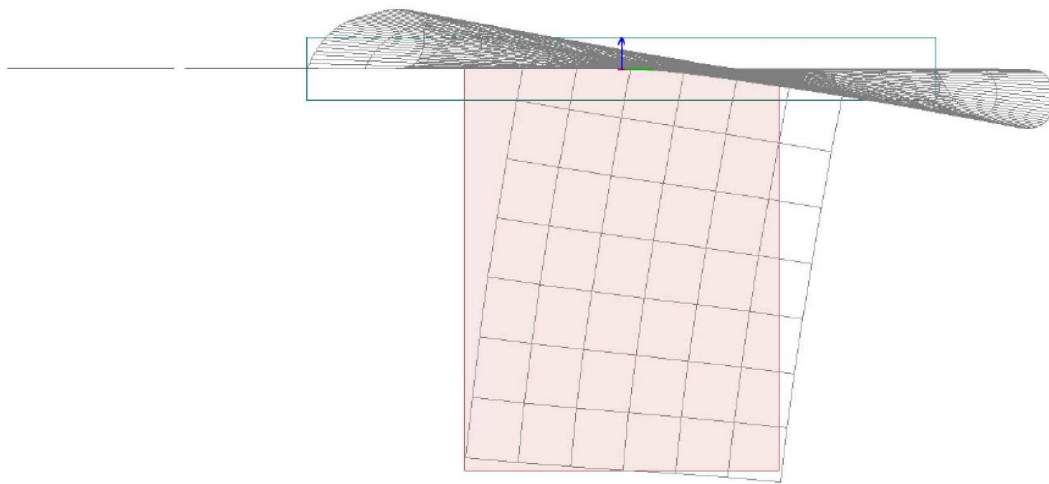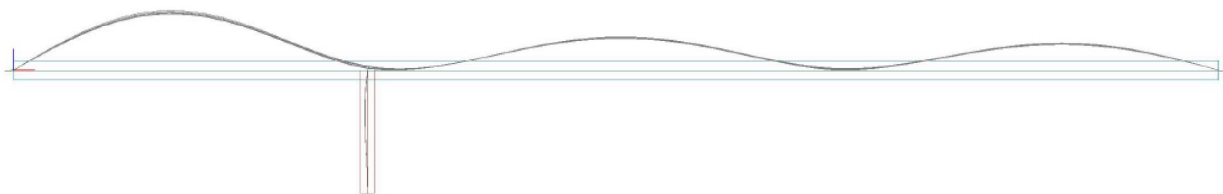
Mode shape 3

Mode shape 4

Appendix B

Data sheet Laser 1: Oclaro 760 nm Single mode VCSEL with Peltier Element and Thermistor in TO510

The following data sheet was retrieved from Oclaro's web side 17th of june, 2014,

link: `http://www.oclaro.com/datasheets/Oclaro%20APC11010108_012012.`
`pdf`

760nm Single mode VCSEL with Peltier Element and Thermistor in TO510

Features:

- Stable single mode operation without mode hops

- Stable polarization

- Highly symmetric Gaussian beam profile

- Wide emission wavelength tuning by temperature and current

- Narrow line width

- High reliability

- Hermetic TO510 package with integrated peltier element and thermistor

- AR coated glass window

- Other wavelength ranges available on request

- RoHS compliant

Applications:

- Oxygen sensing

- FTIR spectroscopy

- Other spectroscopic applications

Oclaro's 760nm VCSELs are designed to meet the requirements for the optical measurement of oxygen concentration levels as well as other spectroscopic applications. The laser emits a single transverse and longitudinal mode with stable linear polarization, small divergence and a highly symmetrical Gaussian beam shape. The hermetically sealed TO510 package features an integrated peltier element and thermistor.

Electro – Optical Characteristics*

Parameter	Symbol	Conditions	Ratings			Unit
			Min	Typ	Max	
Threshold current	I_{th}		1.0	3.0	4.5	mA
Operating current	I_{op}	P_{op} = 300µW	2.0	4.0	6.0	mA
Operating voltage	U_{op}	P_{op} = 300µW		2.4	3.5	V
Differential resistance	R_d	P_{op} = 300µW		130	250	Ω
Emission wavelength	λ	APC1101010801 (P_{op} = 300µW)	758.0		766.0	nm
		APC1101010802 (P_{op} = 300µW)[1]	759.0		766.0	nm
		APC1101010809 (P_{op} = 300µW)	759.0		761.0	nm
		APC1101010810 (P_{op} = 300µW)	763.0		765.0	nm
Maximum single mode output power	P_{sm}	SMSR ≥ 20dB	0.4	0.6		mW
Slope efficiency	η	P_{op} = 300µW	0.1	0.3	0.4	mW/mA
Beam divergence	Θ	P_{op} = 300µW, FWHM		13		°
Linewidth	Δν	P_{op} = 300µW		20		MHz

(1) Excluding wavelengths from 761.5… 763 nm (no O_2 absorption line)
SMSR = side mode suppression ratio; FWHM = full width half maximum
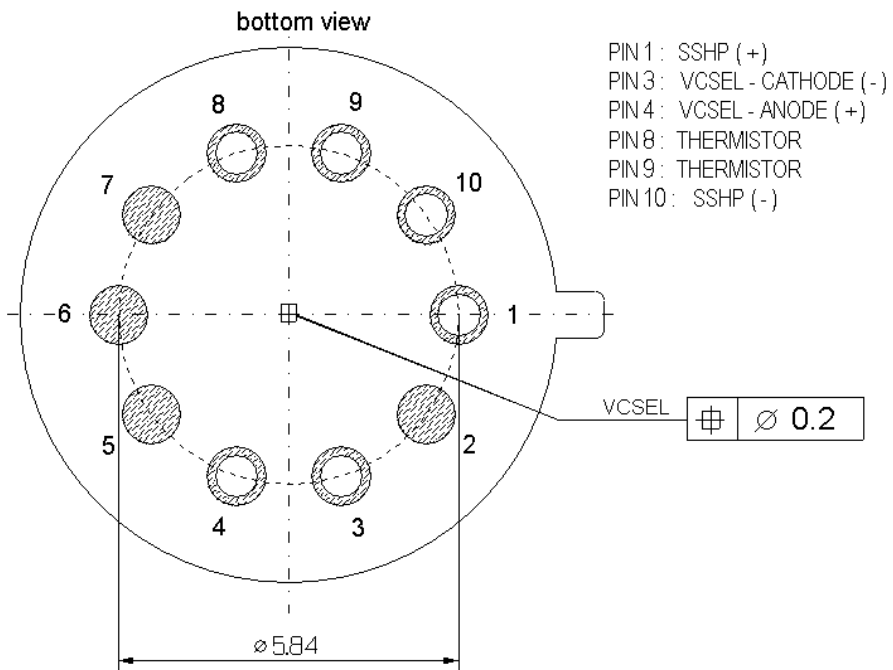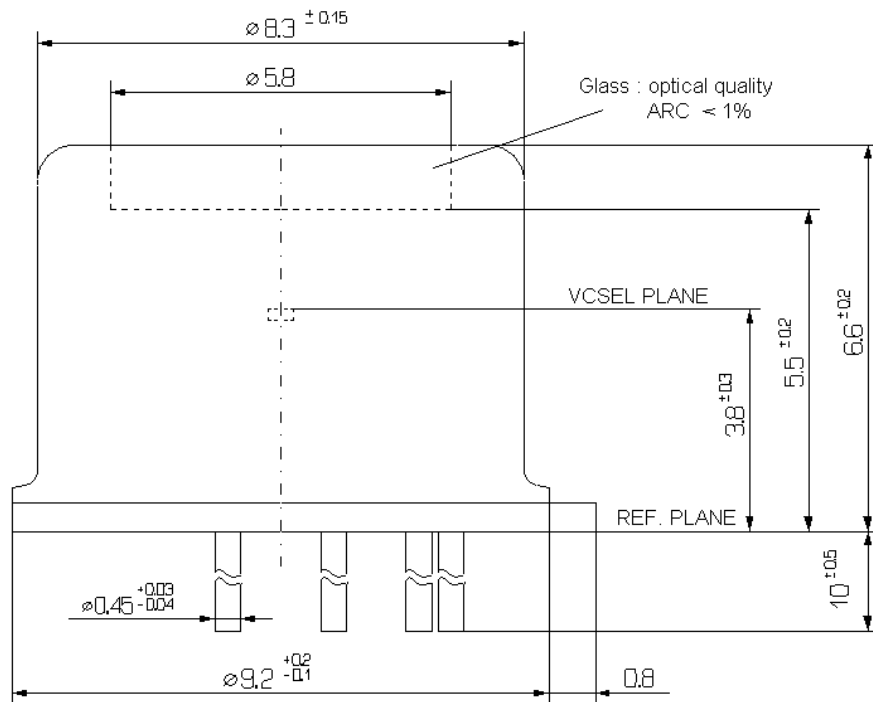
Thermal Characteristics

Parameter	Symbol	Ratings			Unit
		Min	Typ	Max	
Temperature tuning coefficient	δλ/δT		0.055		nm/K
Current tuning coefficient	δλ/δI		0.3		nm/mA
Thermal impedance	Z_{th}		1.5		K/mW
Threshold current variation 0°C - 60°C	$\Delta I_{th,T}$		1.3		mA
Wavelength change over ambient temperature (T=0°C - 60°C, NTC temp. stabilized within 10mK)	δλ/δTamb		0.3		pm/K

*T=25°C unless otherwise noted

Absolute Maximum Ratings

Parameter	Rating	Unit
Optical output power	3	mW
Peak forward current	10	mA
Operating temperature	0 to +60	°C
Storage temperature	-40 to +100	°C
Lead solder temperature (for 10sec)	260	°C
Maximum TEC current	0.6	A
Maximum TEC voltage	0.5	V
Maximum temperature difference across TEC	72	K
Maximum TEC heat load	0.15	W

Mechanical Dimensions and Electrical Connection

bottom view

PIN 1 : SSHP (+)
PIN 3 : VCSEL - CATHODE (-)
PIN 4 : VCSEL - ANODE (+)
PIN 8 : THERMISTOR
PIN 9 : THERMISTOR
PIN 10 : SSHP (-)

RoHS Compliance

Oclaro is fully committed to environment protection and sustainable development and has set in place a comprehensive program for removing polluting and hazardous substances from all of its products. The relevant evidence of RoHS compliance is held as part of our controlled documentation for each of our compliant products. RoHS compliance parts are available to order, please refer to the ordering information section for further details.

Ordering Information:

Product Code	Package	Wavelength
APC1101010801	T0510	758.0…766.0nm
APC1101010802	T0510	759.0…761.5nm or 763.0…766.0nm
APC1101010809	T0510	759.0…761.0nm
APC1101010810	T0510	763.0…765.0nm

Contact Information

www.oclaro.com

Important Notice

Performance figures, data and any illustrative material provided in this data sheet are typical and must be specifically confirmed in writing by Oclaro before they become applicable to any particular order or contract. In accordance with the Oclaro policy of continuous improvement specifications may change without notice. Further details are available from any Oclaro sales representative.

DANGER
INVISIBLE LASER RADIATION –
AVOID DIRECT EXPOSURE TO BEAM
MAX POWER 14 mW / +11.5dBm
WAVELENGTH > 1565 nm
CLASS IIIb LASER PRODUCT
THIS PRODUCT COMPLIES WITH 21CFR 1040.10

INVISIBLE LASER RADIATION
AVOID EXPOSURE TO BEAM
CLASS 1M LASER PRODUCT
Maximum Power 28 mW / +14.5dBm
Wavelength 1565 – 1610 nm
REFERENCE IEC 60825-1 Edition 2.0

BSI
REGISTERED
UKAS
QUALITY MANAGEMENT
003
ISO14001:1996 EMS 504193
TL9000 Rev 3.0 (ISO9001:2000)
FM15040

CAUTION
STATIC SENSITIVE DEVICE
OBSERVE PRECAUTIONS
Caution - use of controls or adjustments or performance of procedures other than those specified herein may result in hazardous radiation exposure.

Appendix C

Data sheet Laser 2: NEL Laser Diode NLK1L5EAYF

The following data sheet was retrieved from NEL in August 2011.

NLK1L5EAYF

1565-1625 nm DFB laser diode in a TO-5 package with thermo-electric cooler.

FEATURES

- ●Wavelength range　　　1565 - 1625 nm
- ●Output power　　　　　10mW

ABSOLUTE MAXIMUM RATINGS(Tsub=25deg.C)

Parameter	Symbol	Ratings	Units
Laser diode reverse voltage	V_R	2.0	V
Laser diode forward current	I_F	225	mA
Operating case temperature	T_{case}	-5 to 70	℃
Storage temperature	T_{stg}	-40 to 85	℃
Peltier current	I_P	0.9	A

ELECTRICAL/OPTICAL CHARACTERISTICS(Tcase=25deg)

Parameter	Symbol	Condition	Min.	Typ.	Max.	Units
Forward voltage	V_F	I_F=30mA		1.2	1.6	V
Threshold current	$I_{(TH)}$	CW		10	20	mA
Chip output power	Φ_e	CW,I_F=70mA	10			mW
Center wavelength	λ_p	CW,Φ_e=10mW		* 2		nm
Spectral linewidth*1	$\Delta\nu$	CW,Φ_e=10mW		2		MHz
Side mode suppression ratio	SMS	CW,Φ_e=10mW	35			dB
Cooling capacity*1	ΔT_{PE}	ϕ_e=10mW,T_{case}=70deg	45			deg.
Peltier current*1	I_{PE}	T_{case}=-5 to 70deg.			0.9	A
Peltier voltage*1	V_{PE}	T_{case}=-5 to 70deg.			2	V
Thermister resistance*1	R	T_{sub}=25deg.		10		kΩ
Far-field pattern	$\theta_{horizontal}$	CW,Φ_e=10mW		25		degree
Far-field pattern	$\theta_{vertical}$	CW,Φ_e=10mW		25		degree

$\Delta T=| T_{case}-T_{sub} |$

* 1 Data is not attached

* 2 Center Wavelength [xxxx]nm.

⚠ **WARNING**

If you plan to use these products in equipment which could endanger lives in the event of a product failure, please consult an NEL engineer before usage. Improper application of these products may endanger life. To avoid possible injury, make certain these products are used in a redundant configuration.

1 These products are subject to export regulations and restrictions set force by the Japanese Government.
2 NTT Electronics Corporation reserves the right to make changes in design,specification or related information at any time without prior notice.
3 The characteristics which are not specified in the data sheet are not guaranteed.
4 The characteristics under the different operation conditions from the ones specified in the data sheet are not guaranteed.

Appendix D

User guide detector 1: Newport 818-BB-21

In this appendix the user guide for the detector Newport 818-BB-21 is added. Unfortunately the was no data sheet or technical description available, but this document was received from Newports scandinavian dealer. This detector was used in the setup when the laser wave length was 760 nm(Laser 1). The user guide was retrieved from Newports website 17th of june, 2014.
Link: `http://assets.newport.com/webDocuments-EN/images/UsrGuide-818-BB_Non-ampPhotodet.pdf`

NON-AMPLIFIED PHOTODETECTOR USER'S GUIDE

Thank you for purchasing your Non-amplified Photodetector. This user's guide will help answer any questions you may have regarding the safe use and optimal operation of your Non-amplified Photodetector.
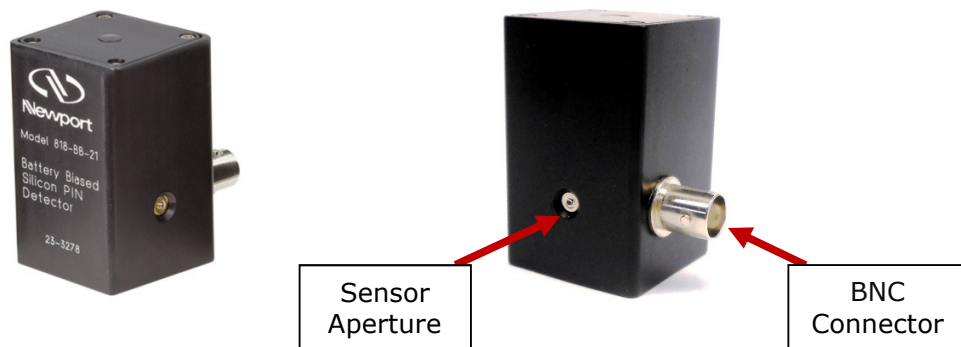
TABLE OF CONTENTS

I.   Non-amplified Photodetector Overview

The Non-amplified Photodetectors contain PIN photodiodes that utilize the photovoltaic effect to convert optical power into an electrical current. Figure 1 below identifies the main elements of your Non-amplified Photodetector.

Figure 1: Non-amplified Photodetector

When terminated into 50Ω into an oscilloscope, the pulsewidth of a laser can be measured. When terminated into a spectrum analyzer, the frequency response of a laser can be measured.

II.   Operation of your Non-amplified Photodetector

A. Caution: Eye safety precautions must be followed when utilizing any equipment used in the vicinity of laser beams. Laser beams may reflect from the surface of the detector or the optical mount and caution must be exercised.

B. Mount the detector to an optical stand by the mounting holes on the bottom of the detector housing.

C. Adjust the voltage of the oscilloscope to 100mV/division before connecting the detector. On models with >3V bias supply, the signal may be large enough to damage the oscilloscope if this is not done.

D. Connect the detector to the oscilloscope using a 50Ω coaxial cable that one meter or less.

E. Use the 50Ω termination input of the oscilloscope. If the oscilloscope does not have a 50Ω input, connect the coaxial cable to a 50Ω terminator and connect this to the oscilloscope's 1MΩ input.

F. After being certain that the damage threshold of the detector is not exceeded, place the detector in the center of the laser beam.

III.   Troubleshooting

A. No signal is seen the first time the detector is used.

1. Be certain that the signal is not high off scale on the oscilloscope.

2. Is the wavelength of the laser within the spectral range of the detector?

3. Has a 50Ω termination input been used?

4. Try moving the detector within the laser beam.

5. Is there enough light (see sensitivity spec on the data sheet) incident on the detector to generate a signal?

### B. A signal has been previously obtained, but not currently.

1. Try steps listed under A.

2. Inspect the active area of the photodiode for any signs of damage.

3. Try a higher input termination on the oscilloscope, but remember to return to 50Ω if this does not work.

4. Test the power supply:

   a. Units with internal batteries will typically operate for several years, but operation with CW or high rep rate lasers can drain the batteries much faster. **If a load is present at the output, current will be drawn from the batteries, so disconnect the BNC when not in use.** Remove top cover to replace the 3V lithium cells with Duracell Model DL2430, positive side down.

   b. Units with an external power supply should at least receive the voltage that is printed on the plug.

5. You can terminate the detector in 1MΩ input of an oscilloscope to obtain a higher output voltage signal but this will decrease the detector's bandwidth by a factor of 5×10^{-5}.

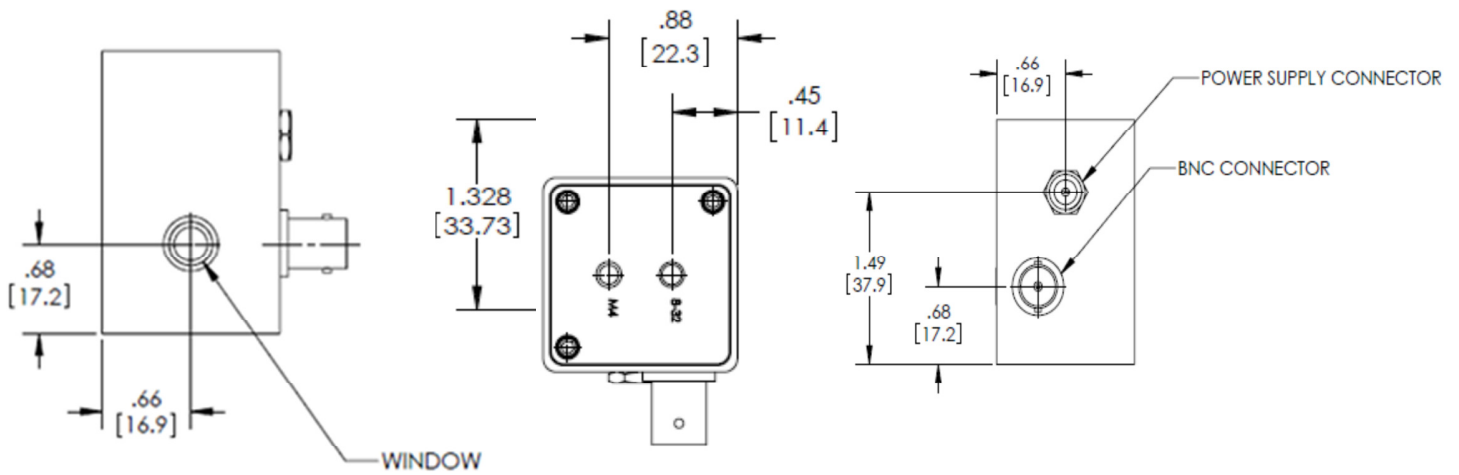### C. Increasing the power incident on the detector does not result in a higher voltage signal on the oscilloscope:

1. The detector is probably saturated. You should lower the power incident on the detector to a level below the saturation point.
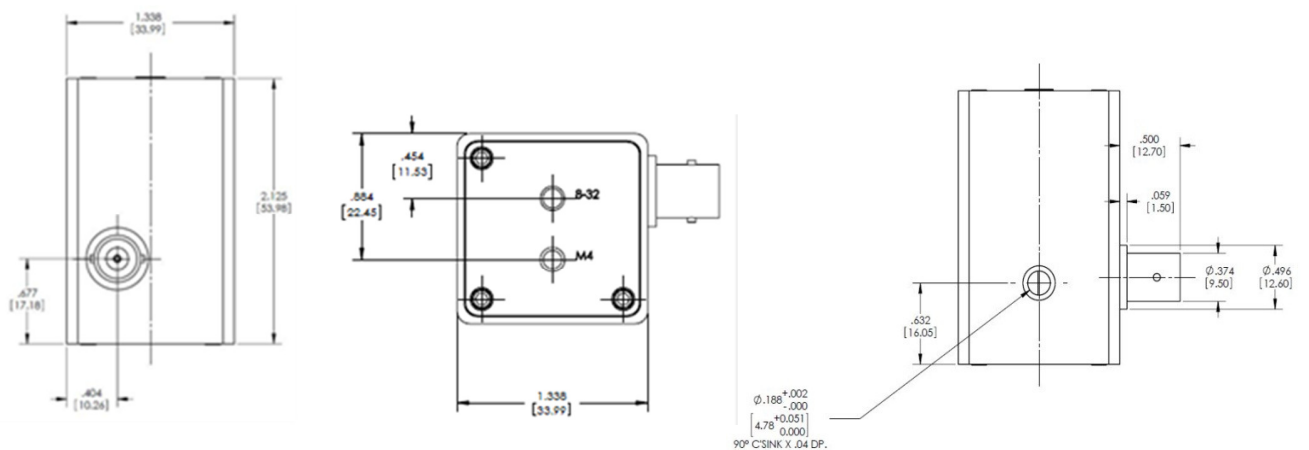
IV. Drawings: Non-amplified Photodetectors

A. 818-BB-20, 818-BB-21 Dimensions:
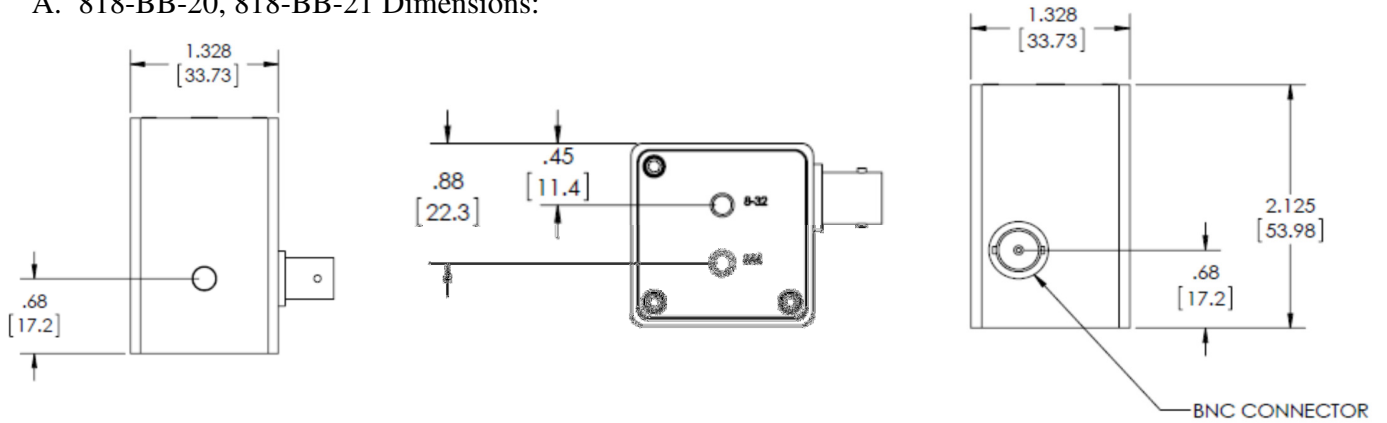

B. 818-BB-22, 818-BB-40 Dimensions:

C. 818-BB-30, 818-BB-31 Dimensions:
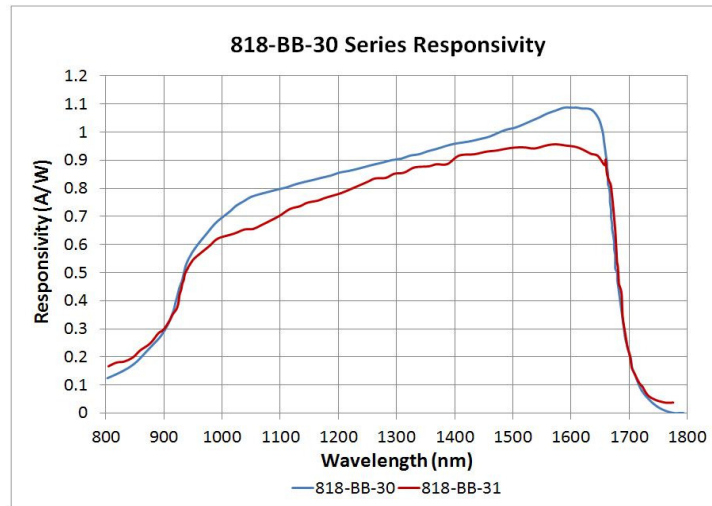
V. Specifications: Non-amplified Photodetectors

A. Biased Silicon Photodetectors:

Part No. (Model)	818-BB-20	818-BB-22	818-BB-21	818-BB-40
Rise Time/Fall Time	<350ps/<350ps	<1.5ns/<1.5ns	<300ps/<300ps	<30ns/<30ns
Responsivity at 830nm	0.12mA/W	0.6A/W	0.47A/W	0.6A/W
Power Supply (VDC)	3	24	9	24
Spectral Range (nm)	350-1100	200-1100	350-1100	350-1100
Bandwidth	>1.0GHz	>200MHz	>1.2GHz	>25MHz
Active Area Diameter	110μm x 55μm	2.55mm	0.4mm	4.57mm
Dark Current (nA)	<0.11	<10	<0.1	<10
Acceptance Angle (1/2 angle)	20^0	50^0	30^0	60^0
Noise Equivalent Power (pW/√Hz)	<0.15	<0.09	<0.01	<0.09
Maximum Linear Rating	CW current: 20mA Energy per 10ns pulse: 20uJ	CW current: 2.5mA Pulse current: 15mA	CW current: 3mA Pulse current: 3mA	CW current: 2mA Optical input: 3mW
Mounting (Tapped Holes)	8-32 or M4	8-32 or M4	8-32 or M4	8-32 or M4
Output Connector	BNC	BNC	BNC	BNC
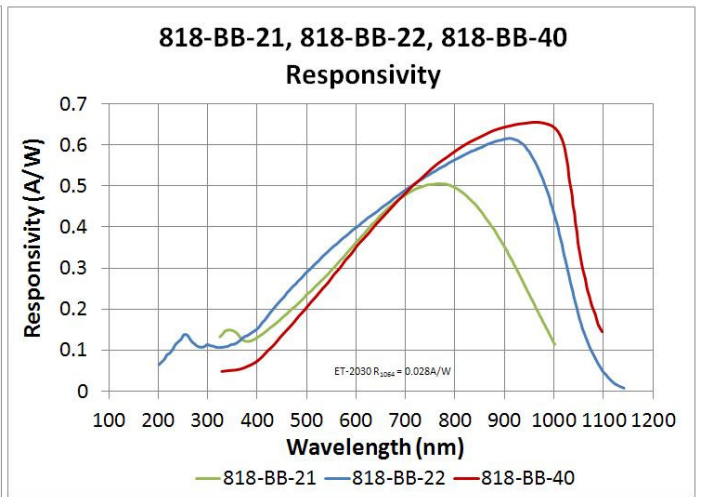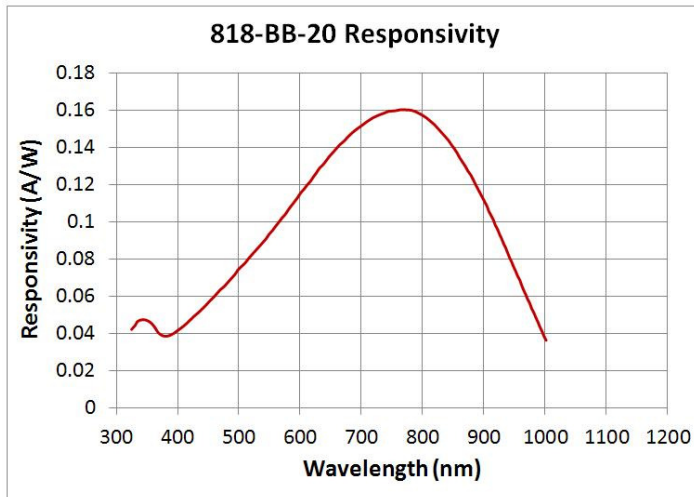
B. Biased InGaAs Photodetectors:

Part No. (Model)	818-BB-30	818-BB-31
Rise Time/Fall Time	<175ps/<175ps	<225ps/<225ps
Responsivity at 1300nm (A/W)	0.9	0.85
Power Supply (VDC)	6	6
Spectral Range (nm)	800-1750	800-1750
Bandwidth	>2GHz	>1.5GHz
Active Area Diameter	100μm	100μm
Dark Current (nA)	<2.0	<1.0
Acceptance Angle (1/2 angle)	20^0	N/A
Noise Equivalent Power (pW/√Hz)	<0.03	<0.02
Maximum Linear Rating	CW current: 5mA	CW current: 5mA
Mounting (Tapped Holes)	8-32 or M4	8-32 or M4
Output Connector	BNC	BNC

818-BB-30 Series Responsivity

VI.   Schematics: Non-amplified Photodetectors
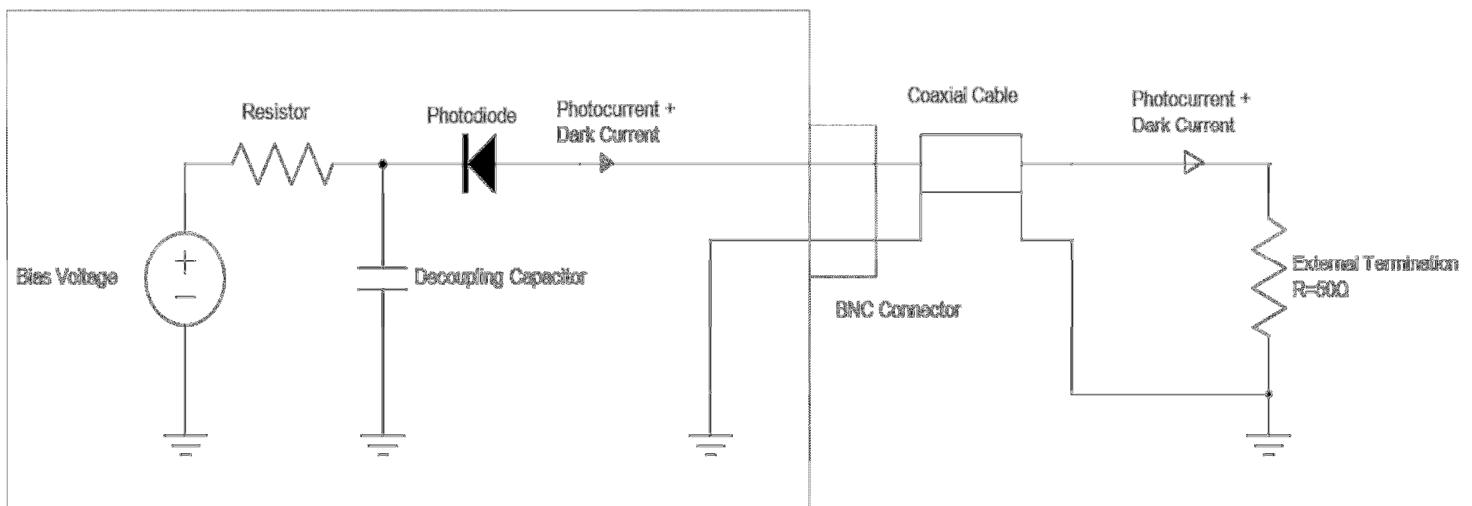
VII.   Glossary of Terms

Bandwidth: The range of frequencies from 0Hz (DC) to the frequency at which the amplitude decreases by 3dB. Bandwidth and rise time can be approximately related by the equation:
Bandwidth ≈ 0.35/rise time for a Gaussian pulse input.

Bias Voltage: The photodiode's junction capacitance can be modified by applying a reverse voltage. The bias voltage reduces the junction capacitance, which causes the photodiode to have a faster response.

BNC Connector: Used to connect the customer's coaxial cable.

Dark Current: When a termination is present, a dark current (nA range) will flow if the photodiode is biased. Disconnecting the coaxial cable will prevent this current from flowing.

Decoupling Capacitor: Maintains bias voltage when fast pulses cause the battery voltage to reduce (this would slow the response time of the photodiode); the capacitor allows the battery to recover to its initial voltage. It also acts as a filter for external power supplies.

Noise Equivalent Power (NEP): A function of responsivity and dark current and is the minimum optical power needed for an output signal to noise ratio of 1. Dark current is the current that flows through a reverse biased photodiode even when light is not present, and is typically on the order of nA. Shot noise (Ishot) is a source of noise generated in part by dark current; in the case of reversed biased diodes it is the dominant contributor. NEP is calculated from shot noise and responsivity. For example, for a responsivity @ 830nm = 0.5 A/W:

$$Shot\_Noise = \sqrt{2qI_d} = \sqrt{2(1.6x10^{-19}As)(20x10^{-9}A)} = 0.08\text{pA}\sqrt{s} = 0.08\text{pA/}\sqrt{\text{Hz}}$$

$$NEP = I_{shot}/R_{830nm} = \frac{0.08\,pA}{\sqrt{Hz}} * \frac{W}{0.5A} = 0.16\text{pW/}\sqrt{\text{Hz}}$$

q = charge on an electron

Photodiode: Converts photons into a photocurrent.

Resistor: Protects the photodiode from excessive current. This could occur if an external power supply was too high in voltage, or if its polarity were reversed; this happens when a customer uses their own power supply.

Responsivity: In amps per watt (A/W), responsivity is the current output of the photodiode for a given input power, and is determined by the diode structure. Responsivity varies with wavelength and diode material.

Rise Time/Fall Time: Rise Time is the time taken by a signal to change from a specified low value to a specified high value. Fall Time is the time taken for the amplitude of a pulse to decrease from a specified value to another specified value. A larger junction capacitance will slow the detector's response time.

Appendix E

Data sheet Detector(Photodiode) 2: Fermionics Opto-Technology FD3000W

The following data sheet was retrieved from Fermionics Opto-Technology on the 4th of August 2014.

Link: `http://www.fermionics.com/fd3000.html`

Large Area InGaAs PIN Photodiodes
diameter of active area=3 mm

DESCRIPTION

Large area, high sensitivity photodiode for use in infrared instrumentation and sensing applications. High spectral response in the region 800 nm to 1700 nm. The photosensitive area is 3 mm in diameter. Planar-passivated device structure.
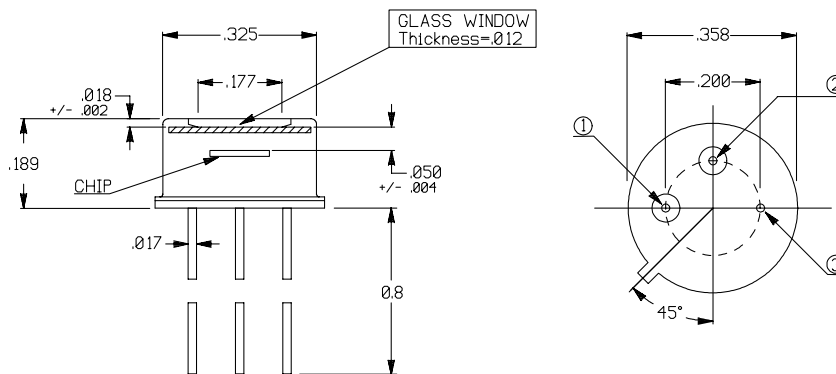
ABSOLUTE MAXIMUM RATINGS (T=25°C)

PARAMETER	RATING	UNITS
Storage Temperature	-40 to +100	°C
Operating Temperature	-40 to +85	°C
Forward Current	50	mA
Reverse Current	10	mA
Reverse Voltage	2	V

OPTICAL AND ELECTRICAL CHARACTERISTICS (T=25°C)

PARAMETER	SYMBOL	TEST CONDITIONS	MIN	TYP	MAX	UNITS
Responsivity	R	λ = 1300 nm	0.80	0.90	-	A/W
		λ = 1550 nm	0.90	0.95	-	
Shunt Resistance ❶	R_S	V_R=0V	1000	2000	-	KΩ
Capacitance	C	V_R=0V	-	750	1800	pF

❶Very High Shunt Resistance devices are available upon request.

DIMENSIONAL OUTLINE

GLASS WINDOW Thickness=.012

.325
.177
.018 +/- .002
.189
CHIP
.050 +/- .004
.017
0.8

.358
.200
① ②
③
45°

(dimensions in inches)

1	ANODE
2	CATHODE
3	CASE

Large Area InGaAs PIN Photodiodes

TYPICAL CHARACTERISTICS

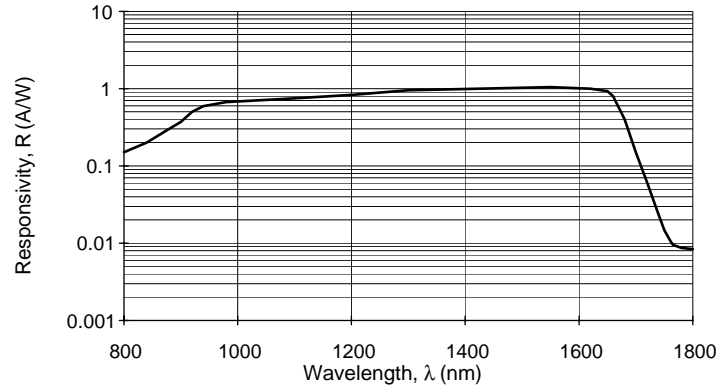**Fig. 1 Spectral Response (R vs. λ)**

Fig. 2 Dark Current vs. Reverse Voltage

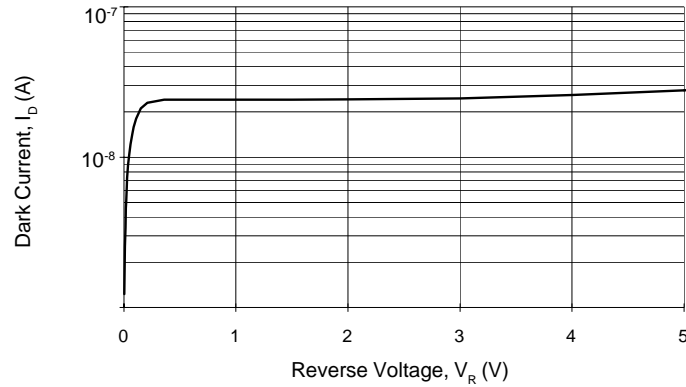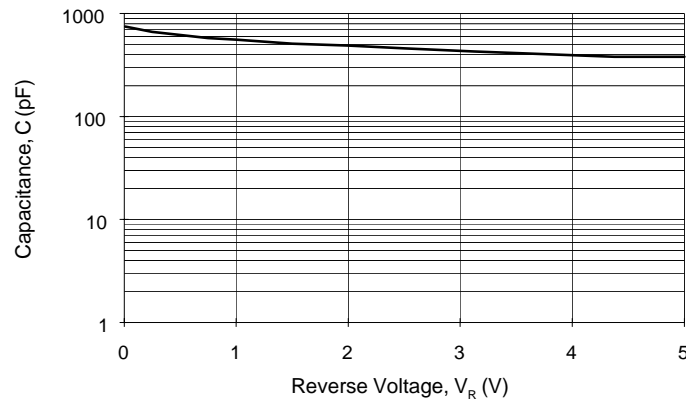**Fig. 3 Capacitance vs. Reverse Voltage**

Appendix F

User guide Optical Spectrum Analyzer: HP 86140A

The specifications presented here were extracted from the user's guide for the spectrum analyser HP 86140A, from page 289-291. The user's guide was retrieved from Link: `http://assets.newport.com/webDocuments-EN/` `images/UsrGuide-818-BB_Non-ampPhotodet.pdf`

Specifications

	HP 86140A and HP 86143A	HP 86142A and HP 86145A
WAVELENGTH		
Range	600 nm to 1700 nm	600 nm to 1700 nm
Span Range (continuously variable)	0.2 nm to full range and zero span	0.2 nm to full range and zero span
Accuracy		
After calibration with internal wavelength reference signal [a]	*±0.025 nm (1510–1570), ±0.035 nm (1570–1640)*	*±0.025 nm (1510–1570), ±0.035 nm (1570–1640)*
After user calibration within ±40 nm of calibration signal [a]	*±0.05 nm*	*±0.05 nm*
After user calibration over full wavelength range [a]	±0.2 nm	±0.2 nm
Absolute accuracy (2 year factory calibration cycle) [a]	±0.5 nm	±0.5 nm
Reproducibility, ≤ 1 minute [a]	±0.003 nm	±0.003 nm
Span Linearity [a,b]	±0.05 nm, for spans <40 nm	±0.05 nm, for spans < 40 nm
Span Linearity (1525 to 1570 nm) [a,b]	*±0.02 nm*	*±0.02 nm*
Tuning Repeatability [a]	±0.003 nm	±0.003 nm
RESOLUTION BANDWIDTH (RBW)		
FWHM (selectable) [a,c]	0.07, 0.1, 0.2, 0.5, 1, 2, 5, 10 nm	0.06, 0.1, 0.2, 0.5, 1, 2, 5, 10 nm
Corrected Resolution Bandwidth Accuracy (using noise markers)[a]		
≥0.5 nm, 1525 to 1610 nm	±4%	±3%
0.2 nm, 1525 to 1610 nm	±6%	±5%
0.1 nm, 1525 to 1610 nm	±12%	±10%

	HP 86140A and HP 86143A	HP 86142A and HP 86145A
AMPLITUDE		
Sensitivity [d]		
600 to 750 nm (no averaging required) [e]	–60 dBm	–60 dBm
750 to 900 nm (no averaging required) [e]	–75 dBm	–75 dBm
900 to 1250 nm (no averaging required) [e]	–75 dBm	–75 dBm
1250 to 1610 nm (no averaging required) [e]	–90 dBm	–90 dBm
1610 to 1700 nm (no averaging required) [b]	–80 dBm	–80 dBm
Maximum Measurement Power		
1525 to 1700 nm	*+15 dBm*	*+15 dBm*
600 to 1000 nm	*+15 dBm*	*+15 dBm*
1000 to 1525 nm	*+12 dBm*	*+12 dBm*
Maximum Safe Power		
Total Safe Power	+30 dBm	+30 dBm
Total Power, within any 10 nm portion of the spectrum	+23 dBm	+23 dBm
Calibration Accuracy at –20 dBm, 1310 nm/ 1550 nm [f]	±0.5 dB	±0.5 dB
Scale Fidelity		
Autorange off, ≤0 dBm [b,g]	±0.07 dB	±0.05 dB
Autorange on, ≤0 dBm [b,g]	±0.1 dB	±0.07 dB
Display Scale (log scale)	0.01 to 20 dB/Div, –120 to +90 dBm	0.01 to 20 dB/Div, –120 to +90 dBm
Amplitude Stability (1310 nm/1550 nm)	±0.01 dB at 1 min *±0.02 dB at 15 min.*	±0.01 dB at 1 min *±0.02 dB at 15 min.*
Flatness		
1290 to 1330 nm [a, f]	±0.2 dB	±0.2 dB
1525 to 1570 nm [a, f]	±0.2 dB	—
1525 to 1610 nm [a, f]	—	±0.2 dB
1250 to 1610 nm [a,h, f]	±0.7 dB	±0.7 dB
Polarization Dependence [a,i,j]		
1310 nm	±0.25 dB	±0.12 dB
1530 nm, 1565 nm	±0.2 dB	±0.05 dB
1600 nm	±0.25 dB	±0.08 dB
1250 to 1650 nm	±0.3 dB	±0.25 dB
1250 to 1650 nm (Option 025)	±0.4 dB	—

	HP 86140A and HP 86143A	HP 86142A and HP 86145A
DYNAMIC RANGE		
In 0.1 nm resolution [a,k]		
1250 to 1610 nm (chop mode on) at ±0.5 nm, ±1 nm, ±5 nm	*−70 dB*	*−70 dB*
1550 nm at ±0.8 nm (±100 GHz at 1550 nm)	−60 dB	−60 dB
1550 nm at ±0.5 nm (±62.5 GHz at 1550 nm)	−55 dB	−58 dB
1550 nm at ±0.4 nm (±50 GHz at 1550 nm)	−52 dB	−55 dB
1550 nm at ±0.2 nm (±25 GHz at 1550 nm)	—	*−40 dB*
MONOCHROMATOR INPUT		
Input Return Loss		
Straight connector (9/125 μm) [l]	>35 dB	>35 dB
PULSE MODE ACCURACY		
Turn On (≥ 2 μs after rising edge)	*< ±0.2 dB (starting from dark)*	*< ±0.2 dB (starting from dark)*
Turn Off (≥ 10 μs after falling edge)	*< ±0.2 dB*	*< ±0.2 dB (30 dB extinction)*
SWEEP		
Maximum Sweep Rate	*40 nm/50 ms*	
Maximum Sampling Rate in Zero Span	*50 μs/trace point*	
Sweep Cycle Time		
50 nm span, auto zero off	*<180 ms*	
50 nm span, auto zero on	*< 340 ms*	
100 nm span, auto zero on	*< 400 ms*	
Full span, auto zero on	*< 1 s*	
Sweep Cycle Time (30 nm span auto zero on)		
−80 dBm sensitivity [d]	*1.8 s*	
−90 dBm sensitivity [d]	*32 s*	
ADC Trigger Accuracy		
Jitter (distributed uniformly)	*<±0.5 μs*	
Trigger Delay range	*2 μs— 6.5 ms*	

Bibliography

[1] Statens Vegvesen. Håndbok N400 Bruprosjektering. *Statens vegvesen, Vegdirektoratet*, 2014.

[2] J. R. Davy. The Barr and Stroud laser rangefinder. *Journal of Scientific Instruments*, 536, 1965.

[3] Garry Berkovic and Ehud Shafir. Optical methods for distance and displacement measurements. *Advances in Optics and Photonics*, 4(4):441, September 2012.

[4] Thierry Bosch. Laser ranging: a critical review of usual techniques for distance measurement. *Optical Engineering*, 40(1):10, January 2001.

[5] François Blais. NRC Publications Archive Archives des publications du CNRC Review of 20 Years of Range Sensor Development. *Journal of Electronic Imaging*, 13(1), 2004.

[6] Helge Storø y. Fibre Bragg gratings and fibre optic structural strain sensing. *Doktor Ingeniøranhandling NTNU*, 22, 1997.

[7] Debashis Satpathi and Arup K. Maji. Electronic shearography for bridge inspection. *Proc. SPIE 2446, Smart Structures and Materials*, 1995.

[8] Ari Kilpela, Riku Pennala, and Juha Kostamovaara. Precise pulsed time-of-flight laser range finder for industrial distance measurements. *Review of Scientific Instruments*, 72(4):2197, 2001.

[9] David George Croft Luck. *Frequency Modulated Radar*. McGraw-Hill, 1949.

[10] Jesse Zheng. *Optical Frequency-Modulated Continuous-Wave(FMCW) Interferometry*. Springer, 2005.

[11] Kjell J. Gå svik. *Optical Metrology Third Edition*. John Wiley & Sons, Ltd., 3rd edition, 2002.

[12] Bahaa E. A. Saleh and Malvin Carl Teich. *Fundamentals of Photonics (Wiley Series in Pure and Applied Optics)*. John Wiley & Sons, 1991.

[13] Koichi Iiyama, Lu-Tang Wang, and Ken-ichi Hayashi. Linearizing optical frequency-sweep of a laser diode for FMCW reflectometry. *Journal of Lightwave Technology*, 14(2):173–178, 1996.

[14] Nadav Levanon and Eli Mozeson. *Radar signals*, volume 20. Wiley-IEEE Press, 2004.

[15] De Yu Zang and James E. Millerd. System for measuring vibration of an object using a coherent optical beam, 1998.

[16] Gail A Massey. Study of Vibration Measurements by Laser Methods. Technical Report January 1968, NASA Rept. No. N 68-14070 (1968) (Natl. Technical Information Service, Springfield, Va. 22151).

[17] Philip C. D. Hobbs. *Building Electro-Optical Systems: Making It All Work*. John Wiley & Sons, Inc., 2000.

[18] Daniel Nordin and K Hyyppä. Finding the thermal time constants of a DFB laser module used in an FMCW ranging system. *Proceedings of the ODIMAP IV Topical Meeting on Distance/Displacement Measurements and Applications, Oulu, Finland*, 2004.

[19] Leilei Shinohara, Julian Asche-Tauscher, Maik Fox, Thorsten Beuth, and Wilhelm Stork. Design and evaluation of a short coherence length laser-based Doppler wind Lidar system for wind energy applications. *Optical Sensing and Detection III*, 9141:91411M, May 2014.

[20] Daniel Nordin and K Hyyppä. Using a discrete thermal model to obtain a linear frequency ramping in a frequency-modulated continuous-wave system. *Optical Engineering*, 44(7):074202, July 2005.